An Assessment of Concentrating Solar Power for Egyptian Locations

Esraa Elmaddah

A thesis submitted to Auckland University of Technology

in fulfilment of the requirements for the degree of

Master of Engineering (ME)

2018

Abstract

Concentrating solar power (CSP) is a promising technology for generating efficient renewable solar energy in countries with high direct normal irradiance (DNI). Egypt, as one of those countries, can very effectively harness the sun's energy for the generation of power, which could have an appreciable impact on Egypt's future energy plans. Nevertheless, the current and planned CSP projects do not match Egypt's solar energy potential. Accordingly, this study examines both the technological and economic aspects of a potential CSP plant in Egyptian locations, in addition to investigating grid integration performance.

A multi-criteria analysis was used in this study to identify and limit the number of the potential sites to three locations to be used as case studies. Subsequently, the System Advisor Model (SAM) simulation package was used to compare the three selected locations in terms of levelised cost of energy (LCOE) and annual energy output. The simulation results demonstrated that a site near Ras Shukeir city in Egypt showed the lowest LCOE with 10.07 US¢/kWh and the best generation performance with an annual energy output of 464.7 GWh.

Based on the output power values of SAM model, load flow studies were performed to assess a CSP system at the site. The load flow solution results showed the values of the expected voltage and voltage angles for each bus for a 24-hour period were acceptable when connected to the grid.

In summary, this work has shown that CSP technology can be adopted on a bigger scale in Egypt, even with the current economic status of the country.

Acknowledgements

Firstly, I am grateful to Almighty God who has given me the strength, guidance and blessings to complete this work.

I would like to express my sincere gratitude to my supervisor Dr Tim Anderson for his guidance, encouragement and supervisory role from the initial to the final level. I would like to thank Professor Tek Tjing Lie for his technical support and valuable input during the work. Without their help and constant feedback, it would not have been possible to complete this thesis.

A very special thank you to the scholarship office team for their continuous support and assistance during my master's journey.

I would also like to say a heartfelt thank you to my wonderful parents, my brother and my sister for always believing in me and encouraging me to follow my dreams. Without them, I would not have had the courage to embark on this journey in the first place.

Lastly, I am grateful for my colleagues and friends especially Shereen and Duaa for their emotional support during my research.

Table of Contents

List of Figures

List of Tables

Attestation of Authorship

I hereby declare that this submission is my own work and that, to the best of my knowledge and belief, it contains no material previously published or written by another person (except where explicitly defined in the acknowledgements), nor material which to a substantial extent has been submitted for the award of any other degree or diploma of a university or other institution of higher learning.

Esraa Elmaddah

September 2018

Chapter 1 Introduction

1.1 Egypt's Energy Profile

Concentrating solar power (CSP) is a promising technology for countries that are located in the sun belt. Egypt, as one of those countries, could utilise the sun's energy for the generation of power. This could have an appreciable impact on the future of energy in Egypt. Many factors have influenced energy consumption in Egypt over the last decade, one of these being the population. As it has increased, reaching 92 million people in 2015 [1], the demand on the national grid has also increased. Furthermore, many new industrial projects have been placing demands on the electricity supply. Electricity consumption in Egypt varies between residential loads, industrial loads, commercial loads, government entities and other public consumers [1]. The combination of population and industrial enterprises has led to a determination to improve and diversify energy sources.

The New and Renewable Energy Authority of Egypt (NREA) has made it known that they want a power plan that includes renewable energy sources, specifically solar and wind energy systems. The total installed capacity in 2012 is shared between fossil fuel and renewable energy, with the renewable energy percentage being less than 12% [2]. This percentage represents current installations of wind power, photovoltaic (PV) systems, CSP plant and hydro power of 550 MW, 15 MW, 20 MW and 2800 MW, respectively. This has led to a suggestion that, in 2020, renewable energy should be at least 20% of supply with an increase in the installed wind power to 7200 MW, PV systems to 220 MW and CSP to 1100 MW. Figures (1, 2) show the total installed energy sources in 2012 and those planned by 2020 in percentages. Furthermore, Egypt has a high direct normal irradiance (DNI), which underpins the country as a strong potential candidate for solar energy systems in general, and CSP technology, in particular, should be viewed as part of Egypt's electricity future.

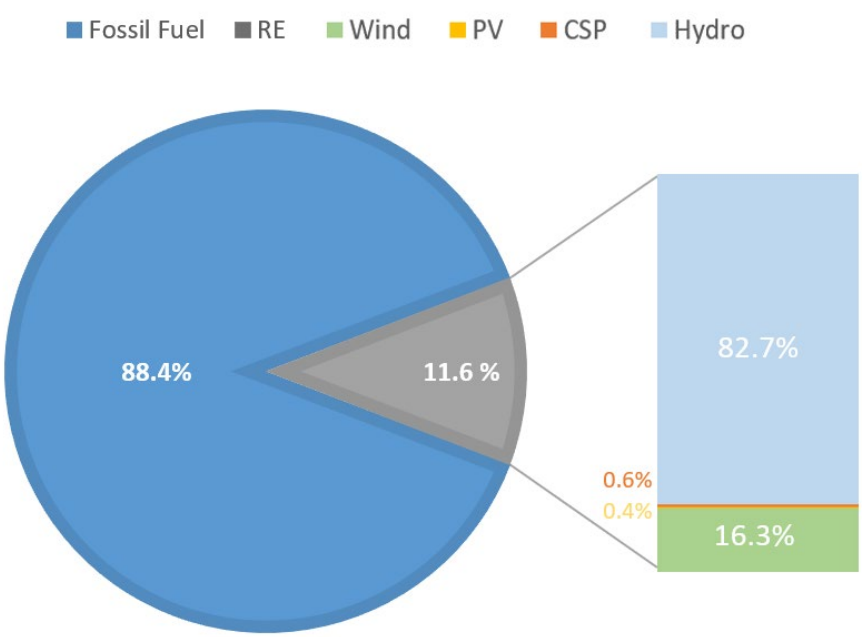

Figure (1): The installed capacity in each sector in 2012 [2].

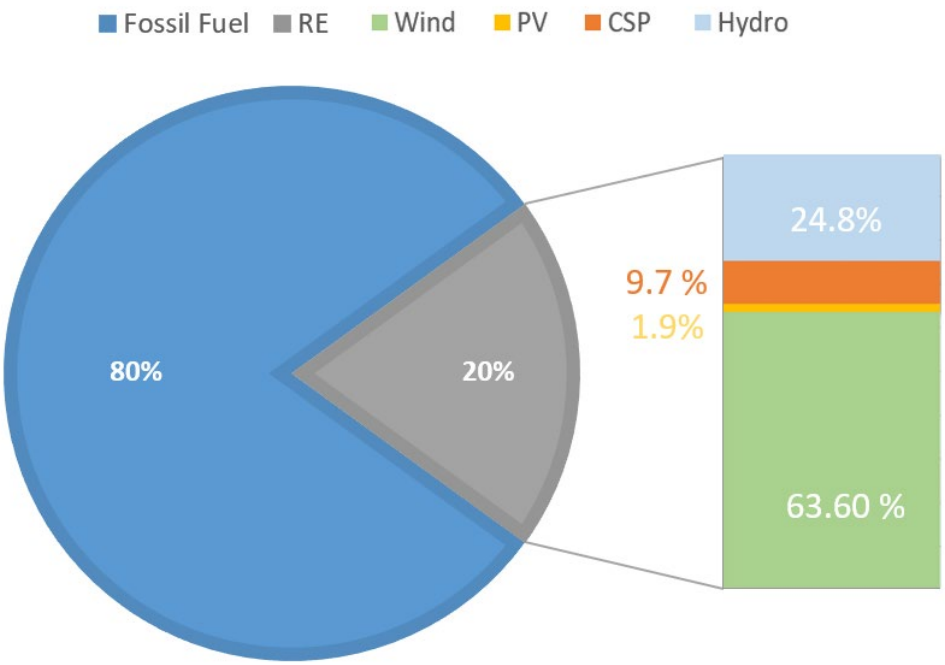

Figure (2): The targeted energy plan by 2020 [2].

1.2 CSP Technology

CSP is a technology that utilises mirrors to reflect and concentrate sunlight to a single point on a receiver where it heats a transfer fluid to a high temperature [3]. This energy is transferred to the next stage where it is used directly to spin a turbine or power an engine that can drive a generator to provide electricity which may be used immediately or stored for later use. At present, CSP systems can be classified into four types according to the technology used: solar power towers, troughs, linear Fresnel reflectors and dishes.

1.2.1 Solar Power Towers

Solar power towers use flat sun-tracking mirrors known as heliostats, which focus sunlight into a receiver at the top of a tower. A heat transfer fluid (HTF) is heated in the receiver, then is used to heat a working fluid that is later utilised in a typical turbine generator for producing electricity as shown in Figure (3). Some power towers use water/steam as the HTF [4], such as the 'Planta Solar 10' in Spain [5]. Other designs use high temperature molten salts or sand-like particles for maximising the power cycle temperature [4]. The Gema Solar Thermo Solar Plant, also in Spain, is a good illustration of this technology [6].

The concentrating solar power tower concept reaches very high temperatures, from 800°C to over 1000°C, and accordingly this increases the efficiency at which the heat is converted into electricity. One attraction of tower technology is that it is extremely flexible which allows the designers to choose from a wide variety of heliostats, receivers, transfer fluids and power blocks, and in addition there are a number of plants which have several towers that provide energy to one power block [7].

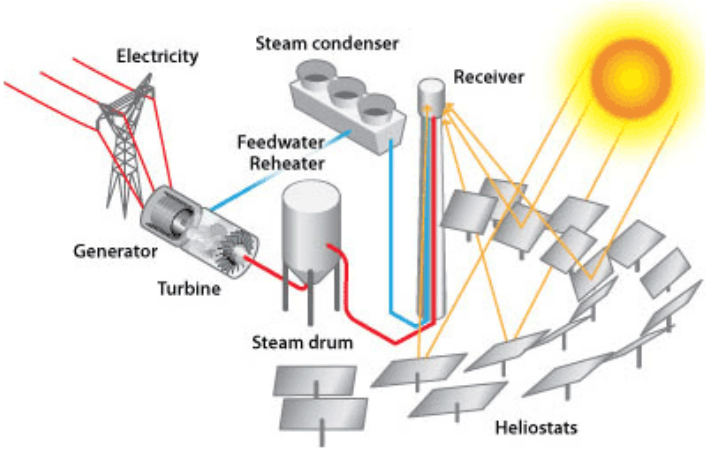

Figure (3): Solar power tower plant [3].

1.2.2 **Parabolic Trough Systems**

Parabolic trough systems are the most common CSP installations to date. According to the National Renewable Energy Laboratory (NREL), approximately 67% of all CSP power plants, including those currently under construction, have adopted this form of power generation [8]. These systems consist of parallel rows of reflectors, curved to focus the sun's rays [7] as shown in Figure (4). These reflectors concentrate the heat from the sun onto an absorber tube, mounted on the focal line of the parabola. The mirrors and the absorber tube move simultaneously, from sunrise to sunset, tracking the sun [9]-[11].

The reflector length can reach 100 m with the curved surface ranging between 5 m to 6 m across. The absorber tubes are made from stainless steel with a selective coating that is responsible for collecting the absorbed heat, the coating being designed to absorb high levels of solar radiation [7]. In addition, these tubes or pipes are insulated in an evacuated glass envelope which results in operating temperatures between 350 °C and 550 °C [9].

Most of the parabolic trough plants that are operating commercially use a synthetic oil as the HTF that transfers the heat from collector pipes to the power cycle. Large numbers of the current parabolic trough plants rely on backup fuel, and no thermal storage is incorporated in these plants. However, newer plants have large thermal storage capacities to allow them to generate electricity after the sun sets [7].

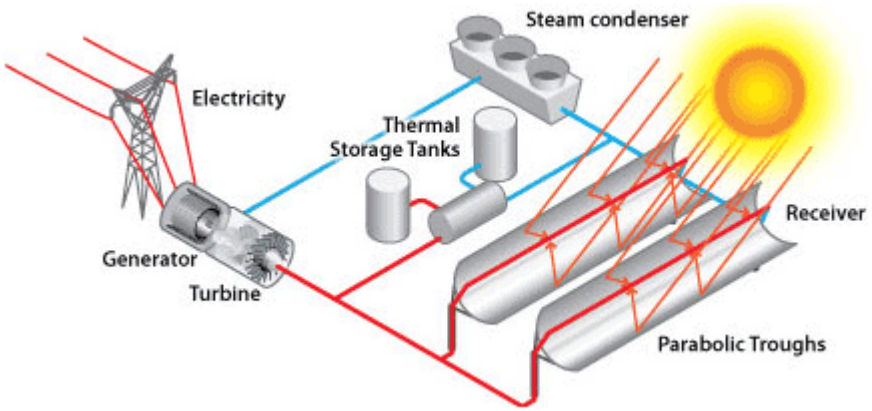

Figure (4): Parabolic trough plant [3].

1.2.3 **Linear Fresnel Reflectors**

Linear Fresnel reflectors (LFRs) resemble the parabolic shape of trough systems but use long rows of flat or slightly curved mirrors for reflecting the sun's rays onto a downward-facing linear fixed receiver, as shown in Figure (5) [7]. One advantage of this technology is that it requires lower investment costs due to the simple design of the flexibly bent reflectors and fixed receivers [7].

However, when it comes in converting solar thermal energy to electricity, LFR plants are less efficient than troughs due to the use of longs rows of mirrors instead of the parabolic design. As the receiver is fixed while the mirrors are rotating, their relative positions change during the day and some light fails to converge and to be focused at a single focal point. This leads to the use of a secondary mirror to reflect back into the receiver tube the sun's rays which have not hit the tube after the reflection of the primary mirrors, and this resulting reflectivity from secondary mirrors reduces the efficiency of the Fresnel reflectors [12].

As for incorporating thermal storage, there have been some attempts made by Germany's Novatec Solar and California-headquartered Avera Solar to develop storage solutions for their Fresnel collectors using molten salt instead of water in order to reach higher temperatures [13]. For Novatec Solar, the attempt succeeded, being tested and demonstrated in the Spanish Errado 1 plant, where the operating temperature reaching 500°C with an electricity yield of 2000 MWh/year [14]. On the other hand, Avera Solar began operation of its molten salt energy storage demonstration plant in 2014 and the results confirmed that using molten salt as the working fluid achieved high temperature during operation as well [15]. As yet, however, this technology is not commercialised properly as it is considered to be a less well-proven technology compared to other types.

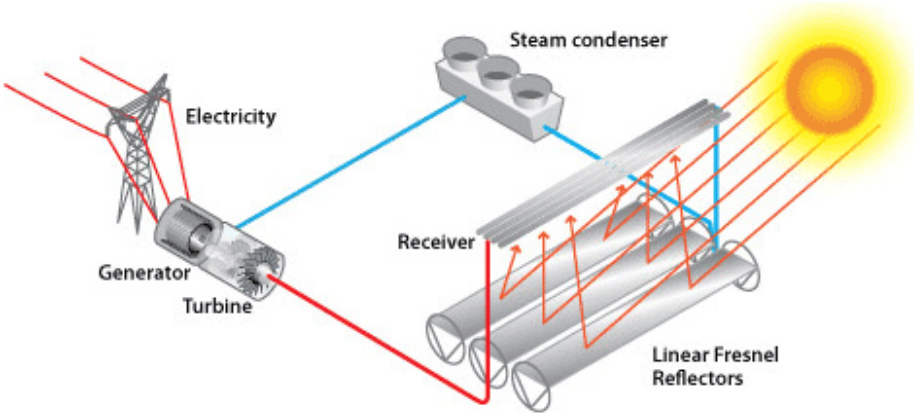

Figure (5): Linear Fresnel reflector plant [3].

1.2.4 **Parabolic Solar Dish**

Parabolic solar dishes focus the sun's rays at a focal point above the centre of the dish. The entire system tracks the sun, with the receiver and the dish moving at the same time [7]. The dishes may have an independent engine/generator at the focal point, as shown in Figure (6). The solar dish provides the highest conversion performance from solar energy to electricity of all the CSP technologies. At the same time parabolic dishes are limited in size to tens of kW capacity, or less, and each dish produces electricity independently. Accordingly, co-location of large numbers of them would be required to create a large-scale plant.

Other CSP technologies have capacities that cover a bigger range starting from 1 MW. The optimal size of troughs, LFRs and towers have capacities which range from 100 MW to 250 MW, depending on the efficiency of the connected power block.

There are many advantages of this dish technology; for instance, the compact size and absence of cooling water and heat transfer fluid. On the down side, the parabolic dish is not compatible with thermal storage and hybridisation, except for the enormously sized dishes [7]. Table (1) shows a detailed comparison between the four technology types.

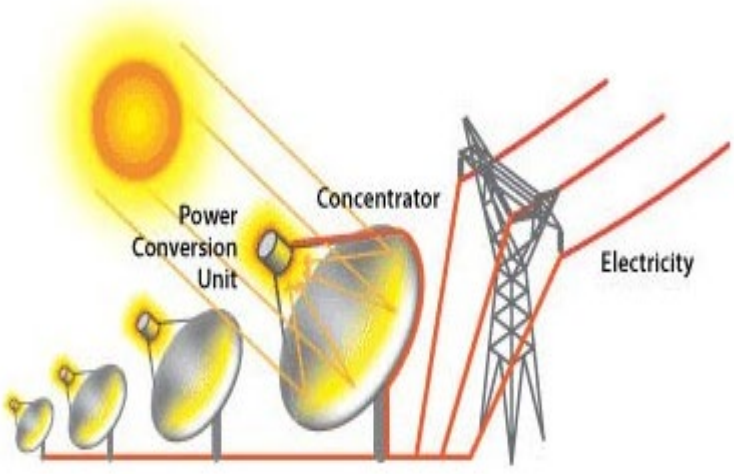

Figure (6): Parabolic dish system [3].

Table (1): Comparison of CSP technologies [7], [16].

Technology	Solar Power Tower	Parabolic Trough	Linear Fresnel Reflectors	Parabolic Solar Dish
Capacity Range (MW)	10 - 100	10 - 250	5 - 250	0.01 - 1
Annual Solar Efficiency	10 - 16 %	10 - 16 %	8 - 12 %	16 - 29 %
Concentration Ratio	600 - 1.000	50 - 90	35 - 170	< 3.000
Land Use Factor	20 - 25 %	25 - 40 %	60 - 80 %	20 – 25 %
Advantages	High efficiency	Long term proven reliability	Simple structure and easy field construction	Compact size, absence of cooling water, high efficiency of power cycle
Disadvantages	High maintenance and equipment costs	Complex structure, limited HTF temperature, flat land and high precision are required	Less efficient, difficult to include storage capacity in the design	High complexity, not compatible with storage except for the large size

1.3 Components of a CSP Plant

For any CSP plant there are three important parts: the solar field, thermal energy storage and power generation systems. The solar field includes solar collectors, receivers, and HTF. Thermal energy storage includes the technologies that have been used for the past and current projects. Lastly, the power generation system includes the power cycle used, which is usually the Rankine cycle, and often includes a backup system for times of low radiation.

1.3.1 **Solar Field**

For CSP technology, solar collectors can be classified into two types: line focus collectors and point focus collectors. Line focus collectors are generally used in either parabolic trough technology or linear Fresnel reflectors. These collectors use highly reflective materials to collect and concentrate the heat energy from solar radiation [17]. In the case

of parabolic trough technology, the collectors are composed of parabolically shaped reflective sections connected into a long trough [18]. As for the point focus solar collectors, this type is usually used in parabolic solar dishes as it has to track the sun across the sky to be effective [17], [18]. These dishes are either working alone or combined into an array to collect more energy from the sun.

The solar receiver is the second part of the solar field which is responsible for absorbing the solar radiation and converting it into heat. It is located at the focal point or along the focal line depending on the type of the collector that has been used. To transform the heat into thermal energy, the heat is transferred through the HTF. In the case of line focus collectors, the receiver is tubular and placed along the focusing line; this type is subjected to lower concentration ratio and medium temperatures. On the other hand, with point focus systems the receiver is more complicated and can take several forms that place absorber surfaces around the focal point, and in addition this type is always subjected to higher concentration ratios with greater temperatures [19].

The third part, the HTF is considered to be a crucial component of any CSP plant as it transfers heat that is concentrated by the receiver to a steam generator. There are multiple types used in CSP plants: for example, water/steam, thermal oil and molten salts [20]-[22]. The function of HTF is transferring heat in a CSP system or storing heat in a thermal energy storage (TES) tank to avoid using a heat exchanger [23]. The characteristics of HTF can be identified as low melting temperature, high thermal stability temperature, high specific heat capacity and low cost [24], [25].

1.3.2 **Thermal Energy Storage**

Thermal storage is a simple concept. During the day, surplus heat is diverted to a storage material (e.g., molten salts); when the plant is required to produce power after sunset, the stored heat is then released into the steam cycle and the plant resumes producing electrical power [7]. Three technologies have been tested and developed since 1985. The first technology type is a two-tank direct system, where the HTF is used as a storage medium. The fluid is stored in two tanks as shown in Figure (7), one tank at high temperature and the other at low temperature. Fluid from the low temperature tank passes through the receiver or solar collector, the solar energy heats it to a high temperature and then it flows to the high temperature tank to be stored; meanwhile the fluid from the high temperature tank goes through a heat exchanger to generate steam for electricity production. The fluid

leaves the heat exchanger at a low temperature and goes back to the low temperature tank [3].

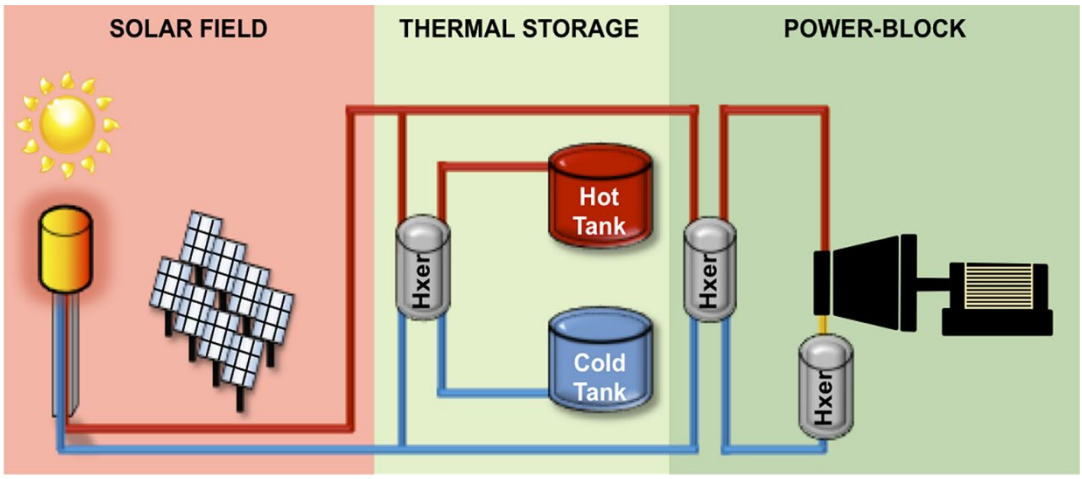

Figure (7): Two-tank direct system of thermal storage [3].

The second type is a two-tank indirect system which operates in a similar way to two-tank direct systems but, in this case, different fluids can be utilised as heat-transfer and storage fluids as shown in Figure (8). These systems are used in plants in which the HTF is extremely expensive or not suitable for being used as the storage fluid [3]. In these systems there is an additional heat exchanger which the storage fluid from the low temperature tank passes through and is heated by the high temperature HTF. Afterwards, the heated storage fluid goes back to the high temperature storage tank, then the fluid leaves the heat exchanger at low temperature and goes back to the receiver where it is heated back again to a high temperature. These systems are usually more costly than other types as they include an additional heat exchanger [3].

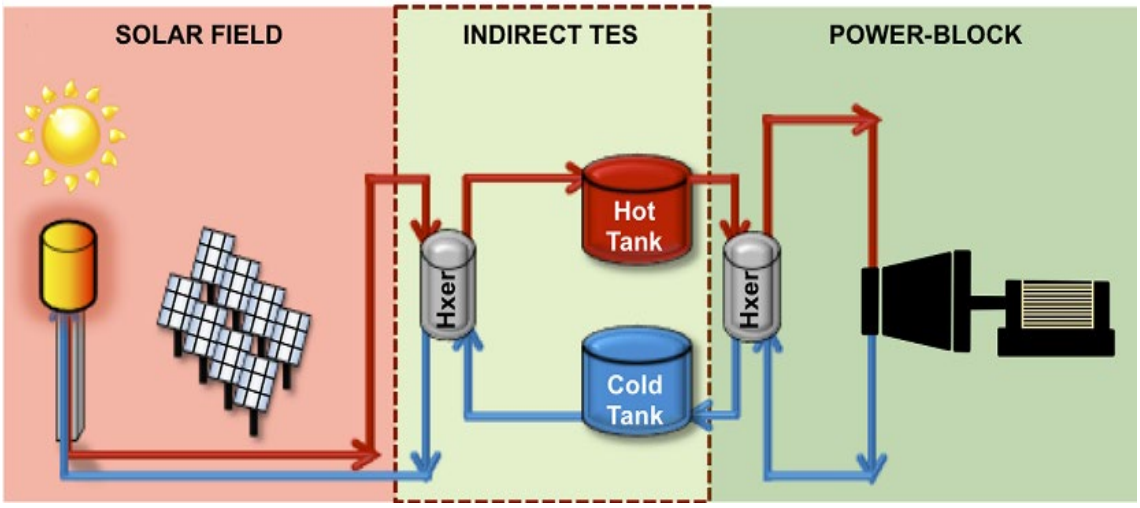

Figure (8): Two-tank indirect thermal storage [3].

The last type is a single-tank thermocline system storing thermal energy in a solid or liquid medium – most often silica sand – placed in one single tank, the hot and cold temperature sections being separated by a temperature gradient or 'thermocline' [3]. The high temperature HTF goes into the top of the thermocline and leaves the bottom part at a low temperature. This storage method has the advantage of depending on a solid storage medium and requiring only one tank, which reduces the cost of the whole system [3]. This type of thermal storage is shown in Figure (9).

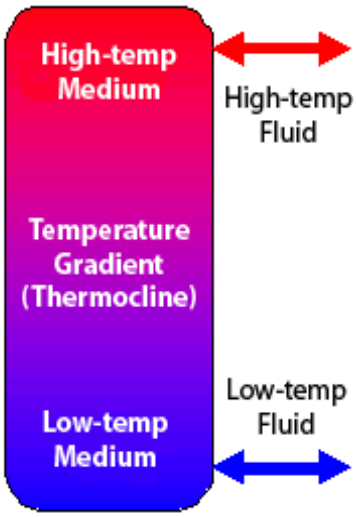

Figure (9): Single-tank thermocline system [3], [26].

1.3.3 **Power Generation System**

The power generation system in any CSP plant includes the power cycle that is used to convert the delivered thermal energy to electrical energy, and the system may include a backup system in case of plant hybridisation. The steam Rankine cycle is most commonly used in power generation for utility scale, for instance, in fossil fuel plants, nuclear, biomass applications and, assuredly, CSP plants. Usually, in CSP plants, the operating conditions are quite different depending on solar resource, storage capacity and ambient conditions [27].

Many CSP plants, whether there is storage provided or not, are usually equipped with a fuel backup system to enhance the capacity of the system, especially during peak and mid-peak hours. In this case, the fuel burners provide energy to the HTF or storage material or to the power block. In some areas where the DNI is not enough for the plant to run completely on solar thermal power, the fuel-powered backup becomes a guarantee of the plant's production capacity at less cost. Another benefit of using fuel burners as a backup system is it increases the conversion efficiency of the solar heat to electric power

by increasing the working temperature level, and for this reason some plants are always in hybrid mode. Adding a solar field to a fossil fuel plant creates what is called an integrated solar combined cycle plant (ISCC). An example of the operation of hybridised solar plant is shown in Figure (10). This example illustrates a system with 30 MW capacity with fuel back up. It can be clearly seen that during the noon hours the extra generated power is transferred to storage to be used later at night.

Also, on the positive side of this solar share is that the cost is relatively low, as the steam cycle and turbine are already in place, and consequently the additional cost will be only due to the components of the CSP plant, which will lead to fuel savings.

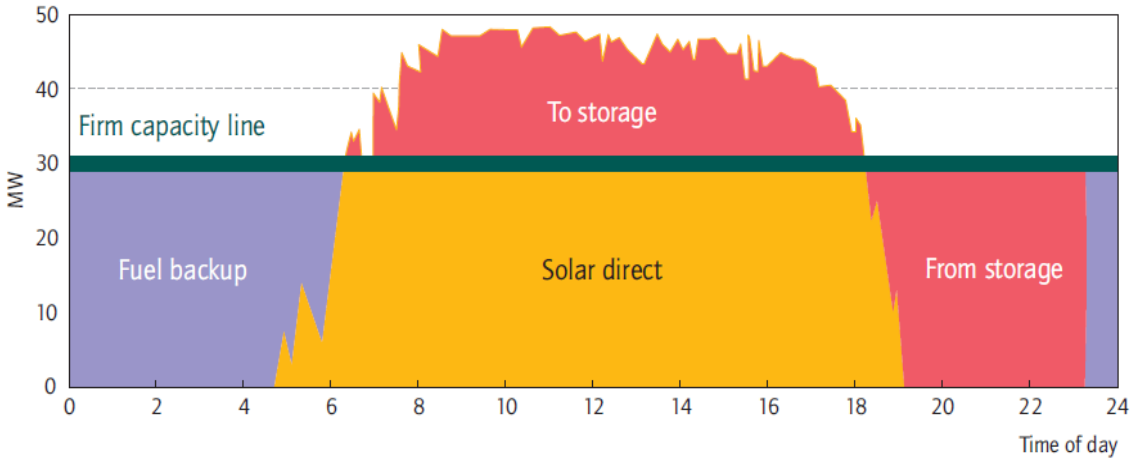

Figure (10): An example of a combination of storage and hybridization in a solar plant [7], [11].

1.4 Overview of CSP Plants Around the World

CSP technology has the potential to be built on a larger scale in the future, and many countries have adopted this type of plant for generating energy, especially countries with high DNI that are suitable for this kind of installation. Spain, for instance, has total of 50 projects installed and under construction; also, the USA has 24 projects both installed and planned. China also has made a huge step in a short time with total of 23 installed and planned projects, based on information on the NREL website [8].

The largest plant in Spain is the Solaben Solar Power Station, also known as the Extremadura Solar Complex, located in Logrosán (Cáceres). It consists of four 50 MW parabolic trough plants: solaben 1, solaben 2, solaben3 and solaben 6. Each plant has a solar field area of 300,000 m^2 and the HTF used is thermal oil. In the USA, the largest CSP plant in the world is the Ivanpah Solar Electric Generating System. This plant started to operate in 2014 with a net capacity of 392 MW. It consists of three separate units,

Ivanpah 1 of capacity of 126 MW and Ivanpah 2 and 3 each with a 133 MW capacity [8]. The plant has a solar field area of 2,600,000 m^2 and uses solar power tower technology backed up with natural gas.

China has made noticeable progress in a short time in depending more on renewable energy in general and CSP in particular. The largest CSP project in the world is currently under construction in China, known as the Huanghe Qinghai Delingha Solar Thermal Power Project. It is planned to have a total capacity of 810 MW after the completion of multiple phases of the project. The first phase started production in 2017 with 135 MW power output. The plant uses water/steam as the HTF, with a storage capacity of 3.5 hours [28].

A summary of some of the biggest CSP projects in various countries is given in Table (2).

Table (2): Summary of some of the biggest CSP plants around the world [8].

Country/ location	**Name**	**Net Capacity (MW)**	**Technology type**	**HTF**	**Thermal energy storage**	**Cooling method**	**Start of operation date**
China/ Delingha	Huanghe Qinghai Delingha Solar Thermal Power Project	810	Solar power tower	Water/ steam	3.5 h / Molten salt/ two-tank indirect	Dry cooling	2017 (under construction)
Spain/ Ciudad Real	Manchasol Solar Power Station	100	Parabolic trough	Diphenyl/ Diphenyl oxide	7.5 h / Molten salts/ two-tank indirect	Wet cooling	2011
Spain/ Córdoba	Palma del Río Solar Power Station	100	Parabolic trough	Biphenyl/ Diphenyl oxide	none	Wet cooling	2010
Spain/ Logrosán (Cáceres)	Solaben Solar Power Station	200	Parabolic trough	Thermal oil	none	Wet cooling	2012
Spain/ Seville	Solnova Solar Power Station	150	Parabolic trough	Thermal oil	none	Wet cooling	2009
UAE/ Madinat Zayed	Shams 1	100	Parabolic trough	Therminol VP-1	none	Dry cooling	2013
USA/ Arizona	Solana Generating Station	250	Parabolic trough	Therminol VP-1 / Xceltherm MK1	6 h/ two-tank indirect (molten salts)	Wet cooling	2013

Country/ location	Name	Net Capacity (MW)	Technology type	HTF	Thermal energy storage	Cooling method	Start of operation date
USA/ Blythe	Genesis Solar Energy Project	250	Parabolic trough	Therminol VP-1	none	Dry cooling	2014
USA/ Ivanpah	Ivanpah Solar Electric Generating system	377	Parabolic trough	Water/ steam	none	Dry cooling	2014

1.5 Related Work and Similar Studies in the Middle East

There have been some studies conducted in the Middle East over the past five years regarding CSP technologies in general and other studies have included more detailed analysis of both the technological and economic aspects of a specific technology or a specific site. Mihoub et al. [29] proposed a methodology for determining the best set of parameters that will ensure the optimum design of future CSP plants with minimum levelised cost of energy (LCOE) and maximal yearly power generation. The term LCOE measures the lifetime costs divided by the energy produced by a system, i.e. the total cost of installing and operating a project expressed in dollars per kilowatt hour (kWh) of electricity generated by the system over its life [30]. This study was based on a planned 50 MW CSP plant in Hassi R'mel city in the south of Algeria.

The study proposed different scenarios for the same site to achieve the lowest LCOE. The System Advisor Model (SAM) [31] was used for simulation of the four different models: the first model did not integrate thermal storage or backup systems, the second model incorporated a backup system without thermal storage, the third model integrated thermal storage without a backup system, and the fourth model incorporated both thermal storage and a backup system. As for the technology selection, there were two cases for each technology type and, for the parabolic trough technology, there were two options for the HTF, therminol VP-1 oil and molten salt, and two scenarios for the cooling method, wet cooling or dry cooling. As for the solar power towers, the detailed configuration options were molten salt as the HTF; external receiver, wet cooling method and molten salt as the HTF; and a cavity receiver dry cooling method.

In addition to the previously mentioned scenarios, the value of the solar multiple was changed in each simulation case. The research recommended the best configuration of variables specifically for the investigated site. The results obtained was different from one technology to another; for example, it was shown clearly that wet cooling was best for Algerian climates regardless of the technology used. The results also showed the

importance of integrating a backup system into the CSP plant, as it led to an increase in annual energy generation in both technologies. In general, the study reached a promising LCOE value of 23.57 US¢/kWh for solar power towers, and 24.12 US¢/kWh for parabolic trough technology. The detailed suggested configuration sets for each technology type are shown in Table (3).

Table (3): The detailed configuration sets that were used in [29].

CSP Plants	Technologies options and configuration	Scenarios
Parabolic trough CSP plant	T1: Therminol VP-1 oil as HTF	S1: Wet cooling technology
	T2: Molten salt as HTF	S2: Dry cooling technology
Solar power tower CSP plant	T1: Molten salt as HTF and external receiver	S1: Wet cooling technology
	T2: Molten salt as HTF and cavity receiver	S2: Dry cooling technology

Another study was conducted in Algeria by Abbas et al. [32]. This research differed from [29] on some points: firstly, it is for a 100 MW CSP plant using only one technology, a parabolic trough; secondly, four sites were included. Furthermore, different climates were chosen for the simulation process (arid, semi-arid and Mediterranean) and the LCOE was calculated in each case. The SAM was also used for the simulation in this research. The study focused on comparing the results obtained for the four selected sites (Tamanrasset, Bechar, Gharadaia, Algeries) as shown in Table (4). The same parameters were used for each case with only one difference, climate. The results clearly showed that the minimum LCOE obtained was in Tamanrasset while the highest was in Algiers. Thus, the study confirmed the idea that the arid regions are the most suitable for installing CSP plants with highest level of annual generated power and lowest cost, while Mediterranean climate regions are the least suitable for CSP technology.

Table (4): Results of the simulation conducted in [32].

Simulation results	Tamanrasset	Bechar	Ghardaia	Algiers
Gross electric output (GWh/y)	465.3	419	251	237
Capacity factor (%)	44.2	39.6	24.5	21.1
Global efficiency (solar to electricity %)	16.4	16	14.2	13.8
Annual water usage (m^3)	84,863	79,830	65,576	62,030

Another study that addressed both the technical and economic sides of solar thermal energy generation was conducted by Purohit and Purohit [33]. This study assessed the technical and economic potential of CSP generation in India. The potential was estimated based on detailed solar radiation and land resource assessment in 591 districts of India. The key parameters for this study were land suitability, favourable solar resource conditions and wind power density over selected regions. The SAM was also used for technical evaluation of CSP technology for the potential sites. The study estimated the CSP potential after considering the suitability of waste land, the annual DNI and the average value of wind power density which is either ≥ 150 or ≥200 W/m^2. The results showed that the LCOE is lower for locations that have high DNI, and, in addition, the results indicated that, at 142 out of 591 locations, using parabolic trough technology is cheaper than central receiver technology at only 18 US¢/kWh.

The first parabolic trough systems were installed in 1912 in Egypt to provide power for an irrigation system and the capacity of this facility was 500 kW [34]. Yet the technology itself with the current changes was not applied until 2011 at the Kuraymat ISCC Plant with an overall capacity of 140 MW (120 MW combined cycle and 20 MW depending on solar energy). The plant uses parabolic trough technology [35]. Table (5) indicates the detailed plant configuration.

Table (5): ISCC Kuraymat plant configuration [35].

Area	130,800 m²
Heat transfer fluid type	Therminol VP-1
Turbine capacity	20 MW
Cooling method	Wet cooling
Cooling method description	Cooling towers
Storage type	None

Regarding the studies that have been conducted in Egypt, Shouman and Khattab [36] presented a road map strategy for introducing CSP into the Egyptian market after investigating the main barriers to financing such a project. In addition, the study also included the peak load and medium load segment of the power supply in Egypt. Furthermore, the study focused on analysing several data sources to compare CSP technologies and LCOE with conventional sources of electricity. The study included the calculation of the cost of generating power from conventional sources and its development in the future, followed by the determination of the cost of CSP with its

development in the future based on the economies of scale after its expected expansion. The results showed that Egypt's CSP potential exceeds 73 000 TWh/year which is one of the highest in the region. The high DNI ranges between 1970 and 3200 kWh/m^2/year and this is available for between 9 and 11 hours per day. In addition, in Egypt there are large areas of unoccupied desert. These findings confirmed the fact that Egypt is one of the most suitable countries for this technology.

All the previous studies discussed thus far considered either or both the technical and economic sides of CSP technology. There are not many studies conducted on CSP performance when connected to the grid, and there was only one study, conducted by Patel et al. [37], that included both modelling and simulation of CSP plants with grid integration. That paper proposed a design for a CSP plant using Simulink with grid integration and made comparisons between CSP and PV technology. The CSP Simulink-based model consisted of different parts with each part representing a process that occurs inside the CSP plant, receiver subsystem, storage system (hot tank and cold tank) and the electric generation subsystem (power cycle). The selected design approach was somewhat similar to PV systems, with some alterations to resemble the same output of a CSP plant. Consequently, the grid integration part of the study was conducted at 22 kV/400 V voltage levels.

1.6 Project Motivation

There are many reasons for selecting CSP technology in general as an approach for this research, and for choosing Egypt as a location for the proposed research project. Firstly, the fact that Egypt is located in the sun belt makes it one of the most convenient locations in the world to adopt this technology on a larger scale. Also, as mentioned previously, Egypt is currently relying more on conventional sources of energy, for instance, oil, natural gas and coal, than on renewable sources. Although Egypt is the largest non-OPEC (Organisation of the Petroleum Exporting Countries) oil producer in Africa, it is also the largest consumer of oil in the whole continent; the country's use of oil represents 20% of Africa's total consumption, which means that consumption has outpaced production since 2010 [38]. Another reason to be considered is the need to establish large numbers of renewable energy projects not only for meeting the growth in energy demand but also as a solution to the worldwide energy crisis as other conventional sources of energy are predicted to run out in 60 years [39].

In addition, as previously stated, Egypt is one of the most convenient countries for renewable energy generation projects, especially solar energy, but still the current and planned renewable energy projects do not match Egypt's renewable energy potential. Meanwhile, from the research perspective, many studies have been conducted in the Middle East in CSP technology but usually these studies combine both technical and economic sides. As stated in the previous section, there is a limited number of published research projects that extend to the next step of grid integration and conduct power flow studies. These various motivations have led to the development of the following research question for this thesis:

Where can a CSP plant be installed in Egypt with low cost and high generation performance?

Chapter 2 Siting Study of Suitable Locations for CSP Technology in Egypt

To install a CSP plant, a siting study needs to be conducted to confirm the selected location's status and determine whether it fulfils the requirements for such a site. Accordingly, this study represents an essential stage before any simulation process can take place.

2.1 Siting Process Requirements

The solar resource is not uniform all over the world, with many differences in levels of irradiance. As CSP technology relies on DNI, this is the first factor that affects the siting selection process. However, in reality a CSP plant cannot be installed in middle of the desert where is no supporting infrastructure; consequently, there are other factors that still matter to the whole selection process and will minimise the total LCOE, for instance, infrastructure including road networks and electrical grid. As a result, siting process requirements for selecting the potential site of a proposed CSP plant are as follows:

- Irradiation data.
- Land resource and investigating the land availability and topography and other factors that are related to geographical features of the selected areas.
- Infrastructure for the national grid and proximity to transmission lines or substations, water resources and access roads.

These requirements were selected based on two studies conducted for site selection or identifying specific zones for CSP technology. The first study, conducted by Tiba et al. [40], used a geographic information system (GIS) for identifying the potential sites for CSP technology in the state of Minas Gerais in Brazil. In addition, the study used a set of requirements adopted from the EM Power Utility Toolkit, which was also used in this research. The second study was conducted by Wu et al. of the International Renewable Energy Agency (IRENA) and the Lawrence Berkeley National Laboratory (LBNL) [41]. In this study multi-criteria analysis developed by the LBNL was used for planning renewable energy zones in Africa. The study followed the same procedures as [40] with the addition of the multi-criteria analysis.

In this present research multi-criteria analysis was also adopted but with some alterations, since it was conducted on a smaller scale instead of covering the whole continent, and with respect to Egypt's current status as a developing country.

2.1.1 **Solar Resource**

Egypt has a DNI ranging between 1900 and 3200 kWh/m^2/year, which is relatively high especially for arid and semi-arid areas. According to Egypt's solar map, as shown in Figure (11), possible locations can be clearly seen on the eastern side of Egypt, especially near to the Suez Gulf and the Aqaba Gulf, where there is an average DNI of 2800 kWh/m^2/year. In addition, the south western region of Egypt could also be considered as a potential location as the average DNI reaches 2600 kWh/m^2/year. However, all these sites need further investigation as DNI is not the only factor that can affect the selection process.

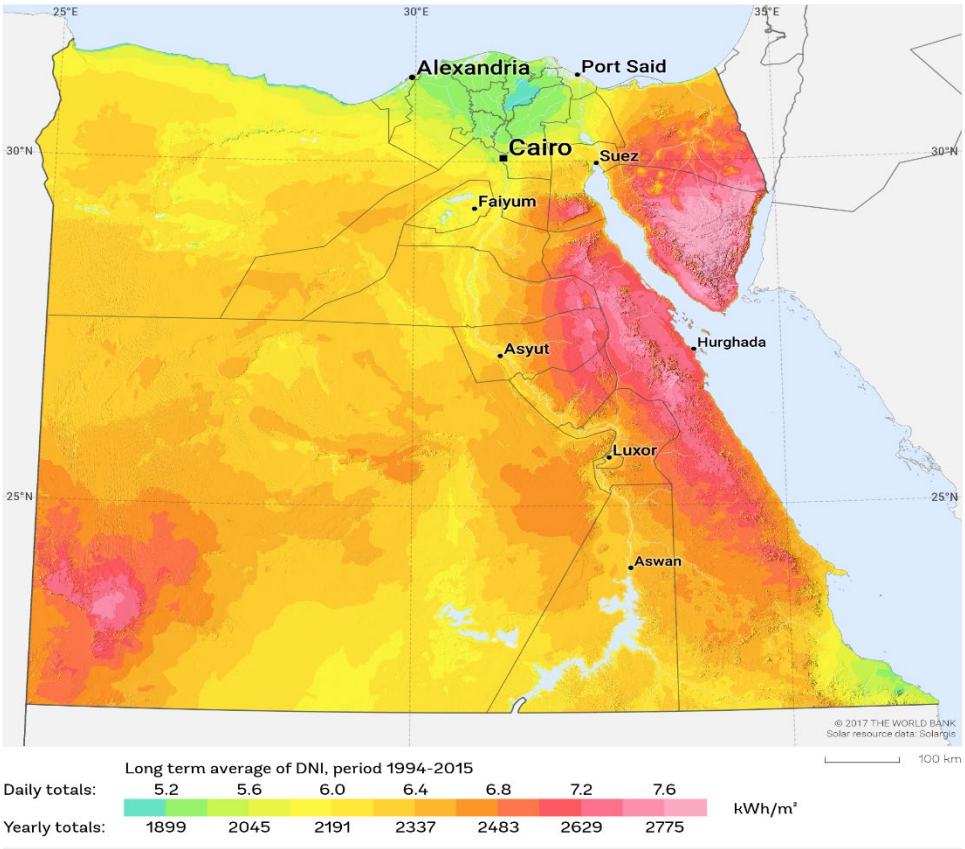

Figure (11) The DNI solar map of Egypt [42].

2.1.2 **Land Resource**

The second factor that affects the selection process is land resource, which includes the land's topography, land availability, land use and land cover (LULC) [40]. As for the topography, the altitude of Egypt ranges from 133 m below sea level in the western desert, to 2,629 m above sea level in the Sinai region [43].

The greater part of the country is covered by the Sahara, which offers many locations and makes it a strong candidate without considering the other affecting factors. Also, the location must be as flat as possible, with obstructions only being allowed where visual angles are less than 100° [40]. The terrain map in Figure (12) shows the elevation levels in Egypt.

As for the LULC, according to the map shown in Figure (13), there are many classes for Egyptian land cover, mainly either barren land, grass land, or urban and built up land. Consequently, in selecting a suitable place, grass land or built up land must be excluded from the selection process to confirm that the final selected sites cannot be used for other purposes, for instance, agriculture, industry and mining or other uses that affect the environment.

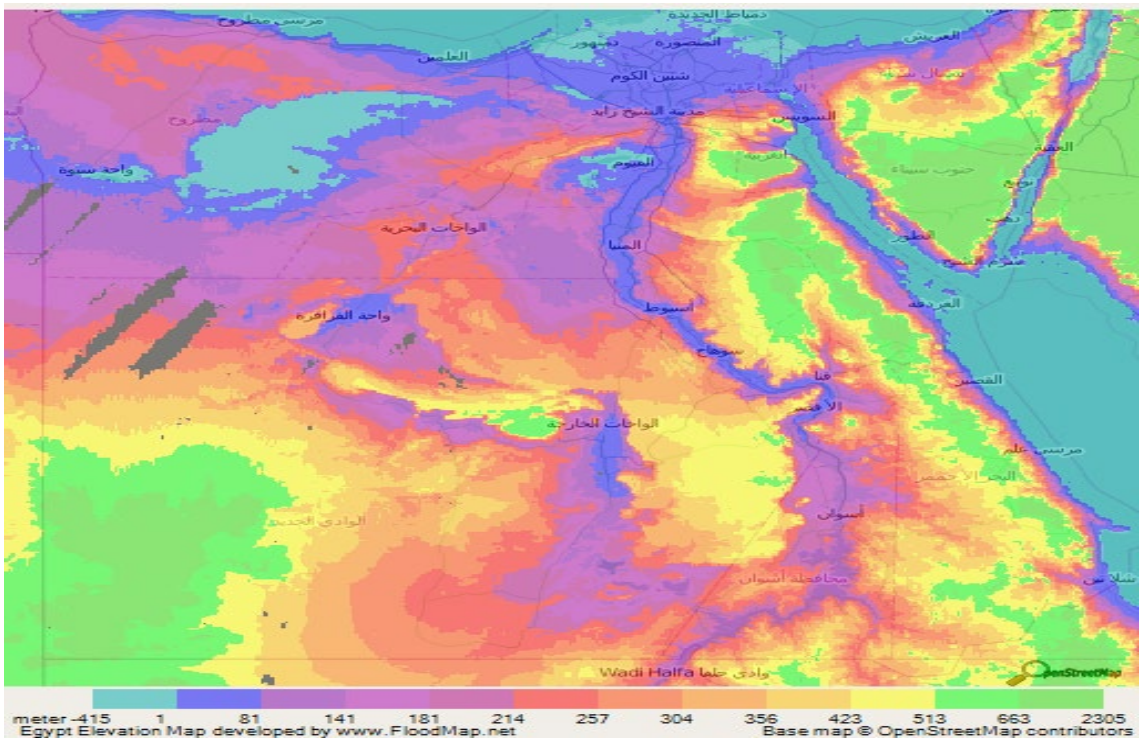

Figure (12): The terrain map of Egypt [44].

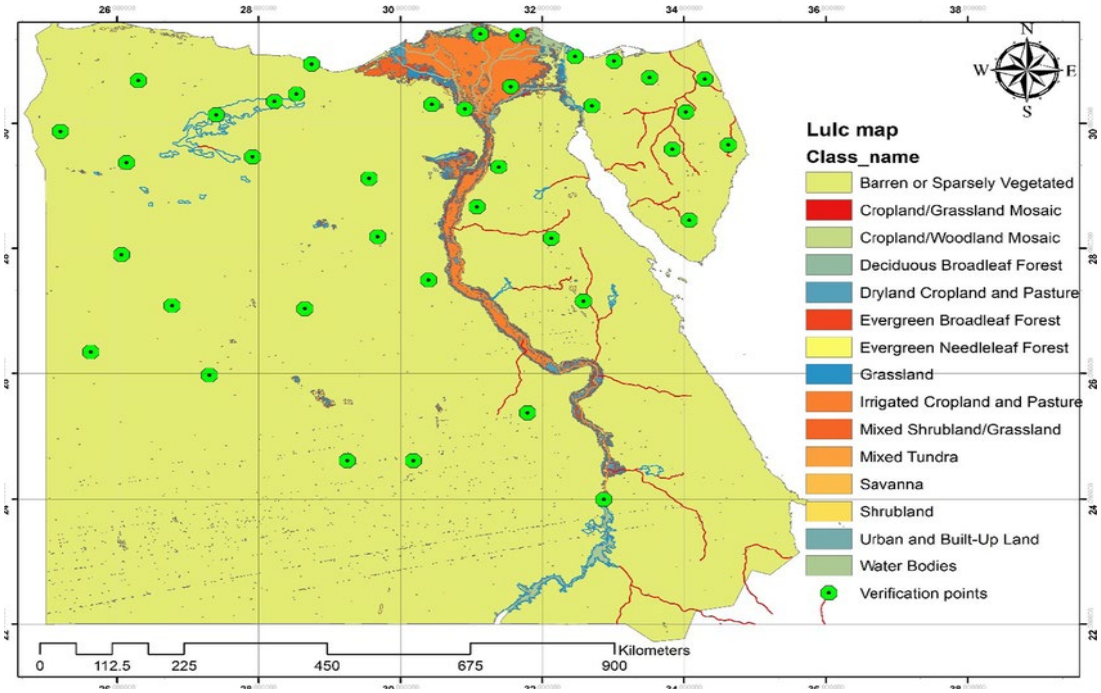

Figure (13): Land use and land cover map of Egypt [45].

2.1.3 **Egypt's Infrastructure**

Egypt's infrastructure is the third factor that can affect the siting process. This includes access road networks as well as water and electricity, as any power plant needs to be installed near to these to reduce the cost of updating the infrastructure. Egypt has a network of over 1 million kilometres including expressways, primary and secondary roads [46]. Most of the primary roads are located near the Nile and populated areas, while there are fewer road networks in arid and semi-arid areas. Figure (14) is a map of the road network.

Figure (14): Egypt's road network [47].

CSP plants also require access to water to make it easier to incorporate this as a cooling method. For example, a 50 MW parabolic trough power plant operating 350 days a year and 10 hours per day uses about 500,000 m^3 of water per year or 1500 m^3/day [40]. This water is required for the cooling towers (90%), steam generation in the power cycle (8%) and cleaning the mirrors (2%) [40]. Egypt has many water resources including seas, a river and some lakes. In addition, according to Egypt's hydrological map, as shown in Figure (15), there are many areas that have access to underground water with moderate productivity, for instance, the Moghra aquifer.

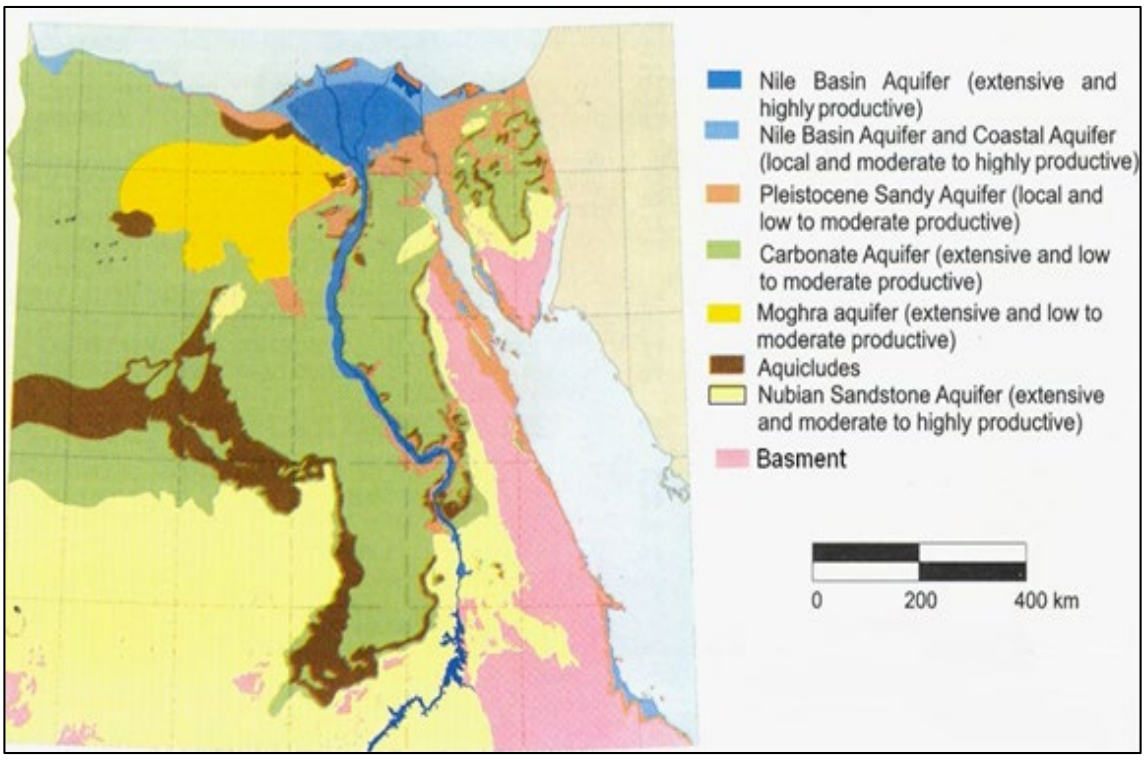

Figure (15): Egypt's hydrological map [48].

Regarding the national electrical grid, Egypt has around 68 power stations with a total installed capacity of 38 857 MW, according to a 2015/2016 Egypt energy report, with peak load reaching 29 200 MW [49]. The total length of medium voltage overhead lines and cables reached approximately 185 000 km in 2016, and the total length of low voltage lines was of the order of 275 000 km [49]. Most of these lines are installed around the Nile valley and across the populated areas, as shown in Figure (16). This affects the selection process as most CSP plants need a large space and are usually in arid and semi-arid areas but ideally with access to the grid. The transmission lines and substations voltage ratings in the delta and river Nile area vary between 110 kV, 220 kV, and 500 kV. Also, the eastern side of the Nile has fewer transmission lines and substations with

the same ratings, while on the western side of the Nile, there is only a limited number of transmission lines and substations which makes this side less favourable in the selection process.

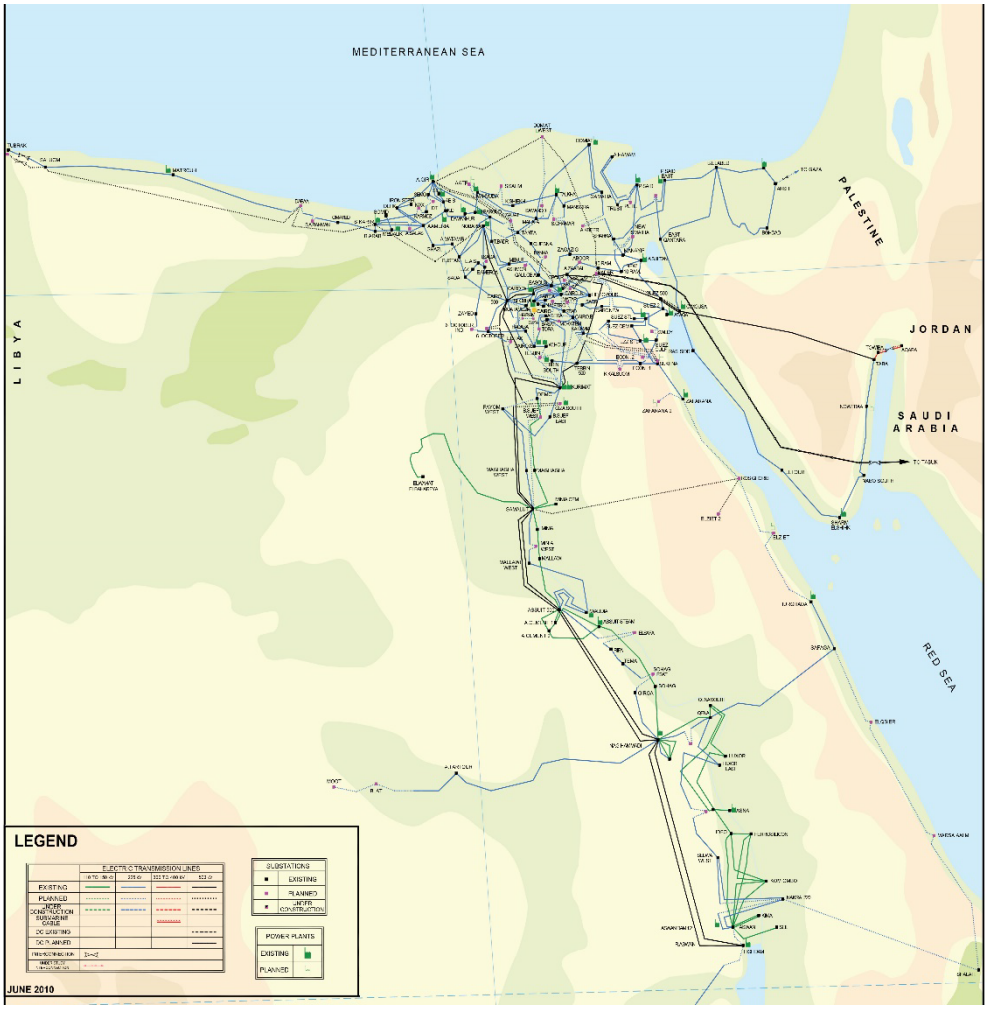

Figure (16): Egypt's national electrical grid [50].

2.2 Preliminary Site Selection Method

Based on the factors mentioned previously, several possible locations were identified using the following criteria:

- Potential sites were selected based on their annual DNI value using the DNI map. Sites were chosen based on them having a yearly DNI of more than 2200 kWh/m^2 per year, as this is the value at which installing a CSP plant is considered feasible [51].
- Only sites with uniform elevation levels were selected, to ensure that there would be minimal site preparation required. As for the land use and cover, barren or sparsely vegetated locations were selected to ensure the CSP was not competing with other land use purposes.

- ❖ The electrical grid network map was used to identify the nearest transmission lines and the connected voltage. Access to the road network was also investigated.
- ❖ The availability of surface water (rivers, lakes and sea), and underground water according to Egypt's hydrological map was examined to evaluate access to cooling water.

In addition to this broad procedure, Google Maps (satellite view) were used to confirm the actual status of each site [52], as shown in Figure (17).

Figure (17): Google Maps feature that was used for site assessment [52].

2.3 Potential Sites

From the preliminary assessment, seven sites were identified for further investigation as shown in Figure (18). A detailed comparison of the potential sites is shown in Table (6).

Site (1)

At latitude 28.06˚ N, longitude 33.25˚ E, this site has an area of 3.74 km^2, and is located near Ras Shukeir by the Red Sea. The DNI in this area is between 2400 and 2600 kWh/m^2/year, and the site is about 1 km from the main road and 1 km from an existing renewable energy plant (wind farm). The site has many additional advantages: it is near to surface water (the Red Sea), it is barren land suitable for construction, the population is less than 100 persons/km^2 [53], and the elevation level ranges from 30 to 141 m, meaning it is readily accessible.

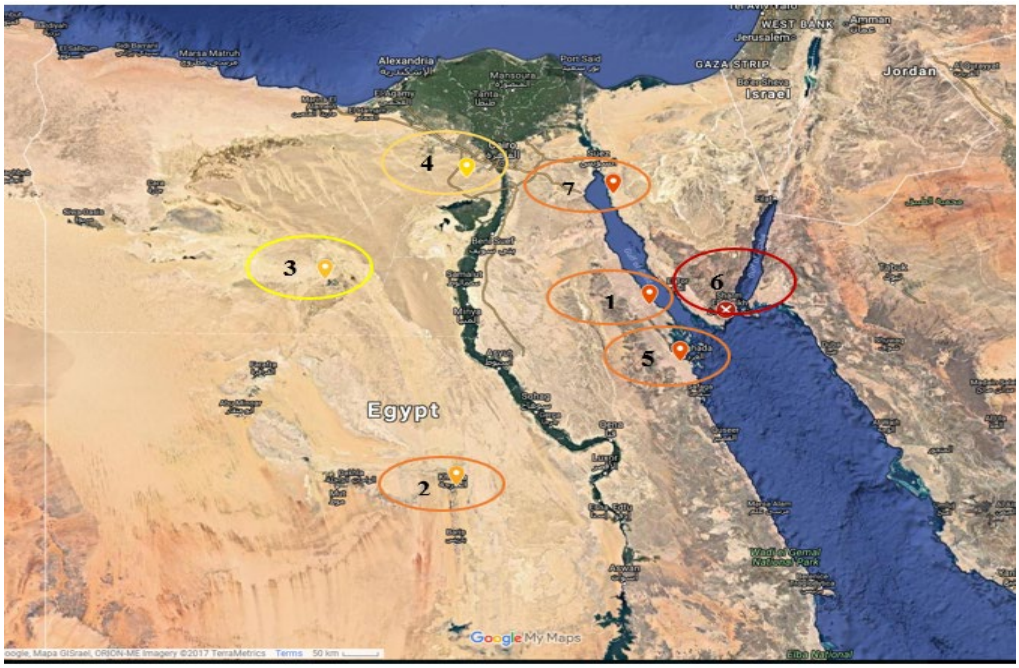

Figure (18): The locations of the seven potential sites.

Site (2)

At latitude 25.5˚ N, longitude 30.61˚ E with area of 3.83 km^2, near Alkharga oasis in the western desert, the site has several benefits: the DNI in this area is between 2200 and 2400 kWh/m^2/year and the site is about 1 km from the main access road in this area. In addition, it sits on barren land, the population is less than 100 persons/km^2 [53], there are large underground water reserves, and the elevation level ranges from 187 to 260 m.

Site (3)

At 28.42˚ N, 28.81˚ E with an area of 4 km^2, near Albahriya oasis in the western desert, this site has several benefits: the DNI in this area is between 2200 and 2400 kWh/m^2/year, the site is about 500 m from the main access road (Siwa-Wahat Elbahriya road). Furthermore, the elevation level is approximately 187 m, the land cover type is barren land, and there is a good potential for underground water according to Egypt's hydrological map.

Site (4)

At 29.83˚ N, 30.75˚ E with an area of 4 km^2, this site is located in the Giza governorate near the 6th of October city. The DNI in this area is between 2100 and 2300 kWh/m^2/year, and the site is about 300 m from the main access road (Giza-Wahat Elbahriya road). This site is a bit different from the other potential sites as it is nearer to the cities and the population in this location ranges from 500 to1000 persons/km^2 [53]. As for the land cover type, it is barren land, and the elevation level is around 187 m.

Site (5)

At 27.27˚ N, 33.66˚ E with an area of 4 km^2, this site is located in Hurghada city where the DNI is between 2400 and 2600 kWh/m^2/year. This site is about 300 m from the main access road (Hurghada two-way road), and has a population less than 100 persons/km^2 [53]. The elevation level ranges between 187 and 260 m, and it is barren land.

Site (6)

At 28.00˚ N and 34.29˚ E, site (6) has an area of 3.55 km^2. This site is near Dahab by the Red Sea with a DNI between 2400 and 2700 kWh/m^2/year. It is about 200 m from the main road and 100 m from the nearest high voltage transmission lines. In addition, the elevation ranges between 187 and 260, and it is barren land. Unfortunately, this area belongs to a protected area, so on closer consideration, was excluded from the selection process.

Site (7)

At 29.61˚ N, 32.75˚ E with an area of 3.55 km^2, this site is near Ras Sedr by the Red Sea. The DNI is between 2400 and 2600 kWh/m^2/year. The site is about 1.3 km from the main road. Furthermore, the distance to the nearest high voltage transmission lines is 1 km, it is barren land, and the population is less than 100 persons/km^2 [53].

Table (6): Comparison between the seven potential sites.

Site	Location		DNI (kWh/m²/ year)	Distance to nearest trans- mission line (km)	High voltage network available (kV)	Road Network (distance to nearest road in km)	Distance to load centres (km)	Elevation (m)	Available Area (km²)	Land use/Land cover	Water sources/ Distance (km)	Population (persons/ km²)
	Latitude	Longitude										
No.1*	28.06˚ N	33.25˚ E	2400: 2600	1	225	0.63	5	30:141	4	Barren land or sparsely vegetated	surface water (Red sea)/ 6.5	Less than 100
No.2	25.5˚ N	30.61˚ E	2200: 2300	1.5	225	1	5	187:260	3.83	Barren land or sparsely vegetated	Underground water /1	Less than 100
No.3	28.42˚ N	28.81˚ E	2200: 2400	10	110:150	0.5	9	187	4	Barren land or sparsely vegetated	Underground water /1	Less than 100
No.4	29.84˚ N	30.75˚ E	2200: 2300	8	225	0.5	18	187:260	4	Barren land or sparsely vegetated	Surface water /35 and underground water /1	500:1000

*This site is near to a newly installed renewable energy (wind farm) plant.

Table (6) continued: Comparison between the seven potential sites.

Site	Location		DNI (kWh/m²/ year)	Distance to nearest trans- mission line (km)	High voltage network available (kV)	Road Network (distance to nearest road in km)	Distance to load centres (km)	Elevation (m)	Available Area (km²)	Land use/Land cover	Water sources/ Distance (km)	Population (persons/ km²)
	Latitude	Longitude										
No.5	27.27˚ N	33.67˚ E	2400: 2600	1	225	0.3	13	187:260	4	Barren land or sparsely vegetated	surface water (Red sea)/9	Less than 100
No.6**	28.00˚ N	34.29˚ E	2400: 2700	0.1	225	0.2	9	187:260	3.55	Barren land or sparsely vegetated	surface water (Red sea)/ 10	Less than 100
No.7	29.62˚ N	32.75˚ E	2300: 2400	1	225	1.3	4	187:260	4	Barren land or sparsely vegetated	surface water (Red sea)/5	Less than 100

** This site is in a protected area. Consequently, it was excluded from the selection process.

2.4 Grading for Potential Sites

Following the preliminary investigation, the different potential locations were graded to limit the number of the selected sites to three. This grading was undertaken using a scoring system based on: the annual DNI, distance to nearest transmission line, distance to the load centre, distance to the nearest road, distance to a water source and, finally, proximity to an existent or planned power plant.

Each of the criteria was given a weight as a part of the final score: DNI as the most important factor, was given the highest value of 50% as it will affect the final cost of electricity produced by the power plant; distance to nearest transmission line was given a weight of 15% as it will also affect the supporting infrastructure cost; distance to the load centre was given a weight of 15%; distance to water resources was also given 15%; and proximity to an existing or planned plant was weighted at 5%.

Each score was graded out of 10; for example, the locations with DNI ranging from 2400 to 2600 kWh/m^2 /year were given a score of 10/10, locations with DNI between 2300 and 2400 kWh/m^2 /year were given a grade of 7/10 and those with the lowest DNI (2200 kWh/m^2 /year were given a 5/10 grade. The detailed grading system is shown in Table (7).

According to the final scoring as shown in Table (8), site (1) and site (5) had the highest scores with 91% and 88%, respectively, making them the most suitable for the proposed plant on the eastern side of the country. Also, on the eastern side, site (7) scored 80%, making it also a potentially viable candidate site. As for the western side of the country, the highest score was site (2) located near Elkharga oasis with an 80% total score which makes it also a suitable site for the proposed CSP plant. However, on a closer inspection it was found that there is an airport nearby, so it was excluded, as the proposed plant might affect air traffic if there were any stray reflections.

Table (7): The grading system.

Data	Scoring system
DNI (kWh/m²/year)	10/10 for 2400:2600 7/10 for 2300:2400 5/10 for 2200:2300
Distance to nearest transmission line (km)	10/10 for 1 7/10 for 5 5/10 for 10
Distance to load centre (km)	10/10 for (1:5) 7/10 for (6:10) 5/10 for (11:15) 3/10 for (16:20)
Distance to water Source (km)	10/10 for (1:5) 7/10 for (6:10)
Proximity to an existing or planned power plant	10/10 for existing or planned 0/10 for the opposite

Table (8): The detailed scores for each site.

Data	Weighing	Site 1	Site 2	Site 3	Site 4	Site 5	Site 6	Site 7
DNI	50%	50.0%	35.0%	40.0%	35.0%	50.0%		35%
Distance to nearest transmission line	15%	15.0%	15.0%	7.5%	9.0%	15.0%		15%
Distance to load centre	15%	10.5%	15.0%	10.5%	4.5%	7.5%	**Excluded**	15%
Distance to water Source	15%	10.5%	15.0%	15.0%	15.0%	10.5%		15%
Proximity to an existing or planned power plant	5%	5.0%	0.0%	0.0%	0.0%	5.0%		0%
Sum	100%	**91%**	80.0%	73.0%	63.5%	**88.0%**		**80.0%**

2.5 Final Selected Sites

After investigating the results of the seven potential sites, only three sites were selected for further investigation and assessment of a possible CSP plant at the sites. These three locations were selected as they had the highest scores: 91%, 88% and 80%; all of them are located in the eastern side of Egypt near the Suez gulf. The other sites may warrant further investigation, but more information would be needed.

The selected sites matched, to some extent, the results that were suggested by the analytical study made by IRENA and the LBNL [41] discussed previously. This analysis identified several places that would be suitable for CSP technology and other renewable energy technologies. Their results showed the possible CSP sites in Egypt, located either near the Suez gulf area and Sinai regions, or a small number of places in the western desert.

2.6 Summary

This chapter investigated and identified the most suitable locations for installing the proposed CSP plant. Initially, seven sites were identified based on direct normal irradiance data, land resource and availability and proximity to water, transmission lines and roads. A detailed site selection method was used to limit the potential sites to just three. This selection method depended on; firstly, a comparison between the seven selected sites in terms of location, proximity to transmission lines, water resources and access roads, high voltage network availability, distance to load centres, elevation, available area, land use/land cover and population density. Secondly, grading the factors that differed in each location based on a scoring system. These final factors were DNI, proximity to transmission lines, load centres, water sources and existing or planned power plant. Accordingly, the three sites with the highest scores were selected to be the subject of further investigation.

Chapter 3 CSP Model Design in SAM and Simulation

Having identified three suitable locations, it was decided to use the System Advisor Model (SAM) to simulate the performance of the proposed CSP plant at the selected locations. For designing the simulation model, some parameters need to be set according to technical details related to the technology used. A specific type of technology should be chosen at this stage, and in this model the parabolic trough type was used for the following reasons:

- This type is the most mature technology among all the technology types.
- Parabolic troughs need less area than other technologies, for instance, Shams 1 in UAE, with only an area of 2.5 km^2, produces 100 MW [54] and Solnova 4 in Spain, with an area of 1.15 km^2, generates 50 MW [55].
- This kind of technology is suitable for Egypt, related to the fact that Egypt is a developing country, therefore it would be better to use the most mature and common technology as it has been already used at the ISCC Kuraymat plant in Egypt [35].

Consequently, the CSP parabolic trough (physical model) was selected as a performance model while LCOE was selected as a financial model.

3.1 Technical Design Parameters in SAM

After selecting the performance model to be employed in the simulation process, the technical parameters for the system itself need to be set accordingly, starting from location and resource to power cycle and thermal storage.

3.1.1 Location and Resource

Based on the coordinates of the three sites, detailed irradiation information was obtained with the help of Meteonorm data sets which provide TMY3 files “Typical Meteorological Year” [56]. These data sets provide calculated annual average values of DNI, global horizontal irradiance (GHI), diffuse horizontal irradiance (DHI), average wind speed and wind direction, in addition to average temperature and elevation. Table (9) shows the values of the weather file data for the first selected site.

Table (9): Annual average weather file data for site (1).

DNI (kWh/m^2/day)	7.58
GHI (kWh/m^2/day)	6.29
Average temperature (°C)	23.7
Elevation (m)	52
Average Wind speed (m/s)	5.7

3.1.2 Solar Field

The first parameter is the solar multiple, which is the ratio between the actual size of a CSP plant solar field and the field size that is needed for driving the turbine at the rated capacity with maximum solar irradiance (1 kW/m^2) [57]. There are two options in the SAM for the solar multiple value, either by setting the value of the solar multiple itself or by selecting the field aperture area. The second method is used as the area of the proposed location is already identified. The total land area used in site selection was taken to be 4 km^2. However, for every type of technology there is a different land use factor, which is the proportion of field aperture area to total land area. Parabolic trough technology has a land use factor ranging from 25% to 40% [16], consequently the maximum field aperture area value was set to 1.1 km^2 or 27.5% of the total area, a value which falls in the advised range.

Another parameter to consider is the number of field subsections. This number decides the location and shape of header piping that conveys heat transfer fluid to the power block that has an effect on determining the heat loss [58]. For this study six subsections were selected, as less than this would create piping problems.

As for partial defocusing during the times when the solar field delivers more thermal energy than the power cycle, there are three possible options: no defocusing, sequenced defocusing and partial defocusing, the first option does not permit partial defocusing as the collectors are either directed to the sun or in stow position [58]. In the second option, partial defocusing is allowed within sequence as collectors can partially defocus by making small adjustments in the tracking angle [58], and the third option allows partial defocusing simultaneously as collectors can partially defocus by the same amount and at the same time [58]. For this work, the third option was selected.

Turning to HTF selection, there are several options representing two kinds of technologies: thermal oil, or molten salt. Therminol VP-1 oil was selected as it is already used in the ISCC Kuraymat plant in Egypt [35], and so can be incorporated in the proposed CSP plant relatively free of risk. This HTF has a minimum operating temperature of 12 °C and a maximum operational temperature of 400 °C [31].

3.1.3 Collectors and Receivers

The solar collector is the most important component in any CSP plant as it is responsible for tracking during the day. This part includes the mirrors, supporting structure, and receivers. The selected collector was the LUZ LS-3 technology. These reflectors are made of hot-framed mirrored glass panels, supported with a truss system. The width of parabolic reflectors (aperture) is 5.76 m and the overall collector length is 95.2 m [31]. These collectors have a high level of generated energy as the high mirror quality permits 97% of the reflected rays to be incident on the linear receiver [59]. The mirrors are manufactured from a low iron float glass with a transmissivity of 98% which is silvered on the back and later covered with various protective coatings. The parabolic shape is obtained by heating the mirrors on precise parabolic moulds in special ovens [59].

As for the receivers, Siemens UVAC 2010 (Universal Vacuum Air Collector) was selected. It is a 4 060 mm long stainless-steel tube with a selective coating outer diameter of 70 mm and a borosilicate anti-reflective glass envelope with an outer diameter of 115 mm [60]. The most important benefit of this receiver is its high solar absorption, which is at least 96% [60].

3.1.4 Power Cycle and Thermal Storage

For the power cycle, the trough physical model in the SAM includes a power block that converts thermal energy generated from the solar field and an optional thermal energy to electrical energy system using a conventional steam Rankine cycle power plant. The model also can include a backup fossil fuel boiler that heats the HTF before it enters the power cycle when there is not enough solar energy to drive the power cycle at its rated capacity. In the proposed system, no backup system was specified as it was assumed that the plant will operate solely on solar energy. The plant design gross output was 111 MW, with an estimated net output of 100 MW, and the proposed cooling method was air cooled, with water only to be used for washing the mirrors.

The thermal energy storage (TES) unit needs to be incorporated into the system as it will store the heat to be used later for generating power when there is little or no sunlight. The full load hours of the storage system are estimated to be eight hours, based on cost and performance considerations. More than eight hours will cost more, and this is the minimum time that allows the energy to cover a reasonable part of the peak load.

Therminol VP-1 was selected to be the storage HTF, as it had been also selected as the HTF of the system. A thermal dispatch control schedule is a part of the thermal storage parameters. This schedule controls the calculation of the energy flows between the solar field, thermal energy storage system, power block, and fossil fuel fraction, though, as there is no backup system in this system, the value of this fraction will be set to zero.

There are three different more fraction values in the schedule that should be set, other than the fossil fuel fraction. The first fraction is storage dispatch fraction with solar, which represents the least amount of energy in storage which will be delivered to the power block in case of incident solar energy [31]. For example, if the value of this fraction is one, it means that the TES will not be used to ensure the maximum power output and the system will be only dependent on solar energy generated at that time. And if the value of the fraction is zero that means that TES will be incorporated in the generation process to ensure maximum output (rated capacity).

The second fraction value is storage dispatch without solar. This fraction indicates the least amount of energy in storage which will be delivered to the power block in case of night time and zero means the opposite, as TES will be used for ensuring the maximum output is reached [31]. The third fraction value is the turbine output fraction, this value representing the percentage of the rated capacity of the turbine output. Here one means 100% of the nameplate capacity and any other value below one represents a percentage of this capacity [31].

Setting these values is dependent on two factors: the peak load and DNI profile. The peak load profile in Egypt, as shown in Figure (19) [49], was interpreted as a percentage to be followed as a pattern, the peak represents 100% and during other hours of the day it was considered as a percentage of this peak. For instance, according to the annual report the peak value is nearly 30 000 MW (100% of the peak load) and the load profile from 2 pm to 7 pm is around 25 000 MW (80% of the peak load). The second factor is dependent on the DNI profile for the site and shows the expected direct irradiance from sunrise to

sunset. Figures (20, 21), respectively, indicate the dispatch mode and the monthly output of the dispatch mode compared to the DNI during the day.

A summary of all the technical parameters that were used in the SAM simulation model is shown in Table (10). The simulation setups for the three selected locations are shown in detail in Appendix A.

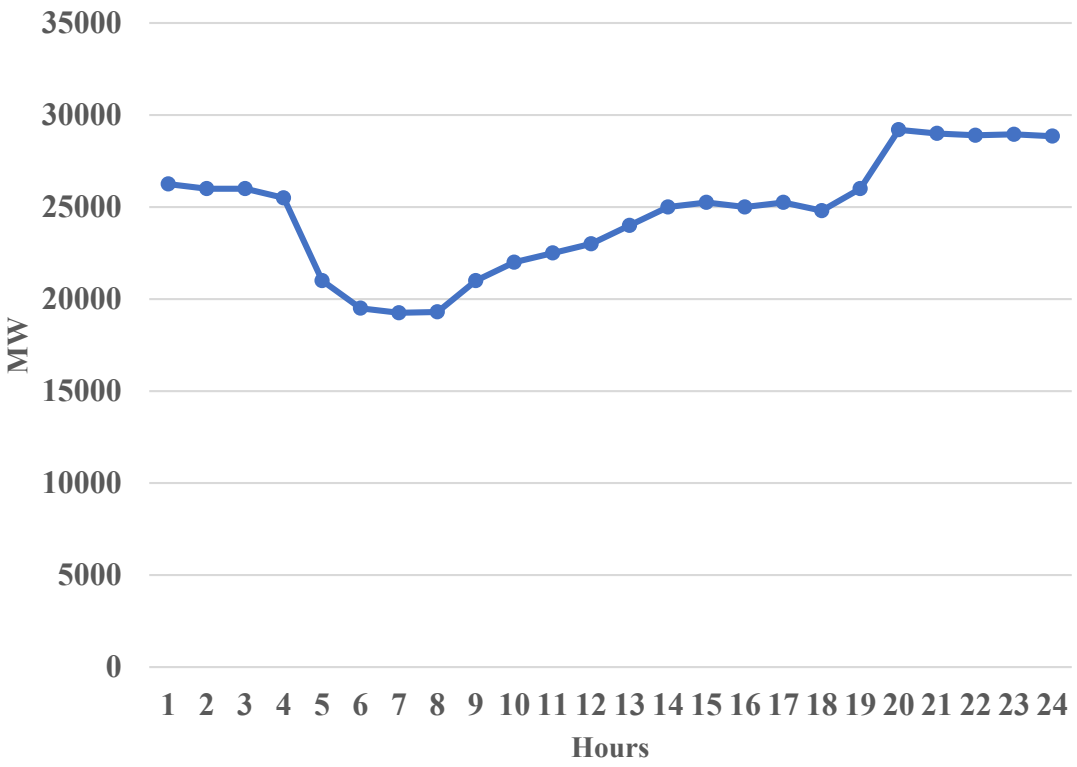

Figure (19): Peak load for 2015/2016 according to annual report of Egyptian Electricity Holding Company.

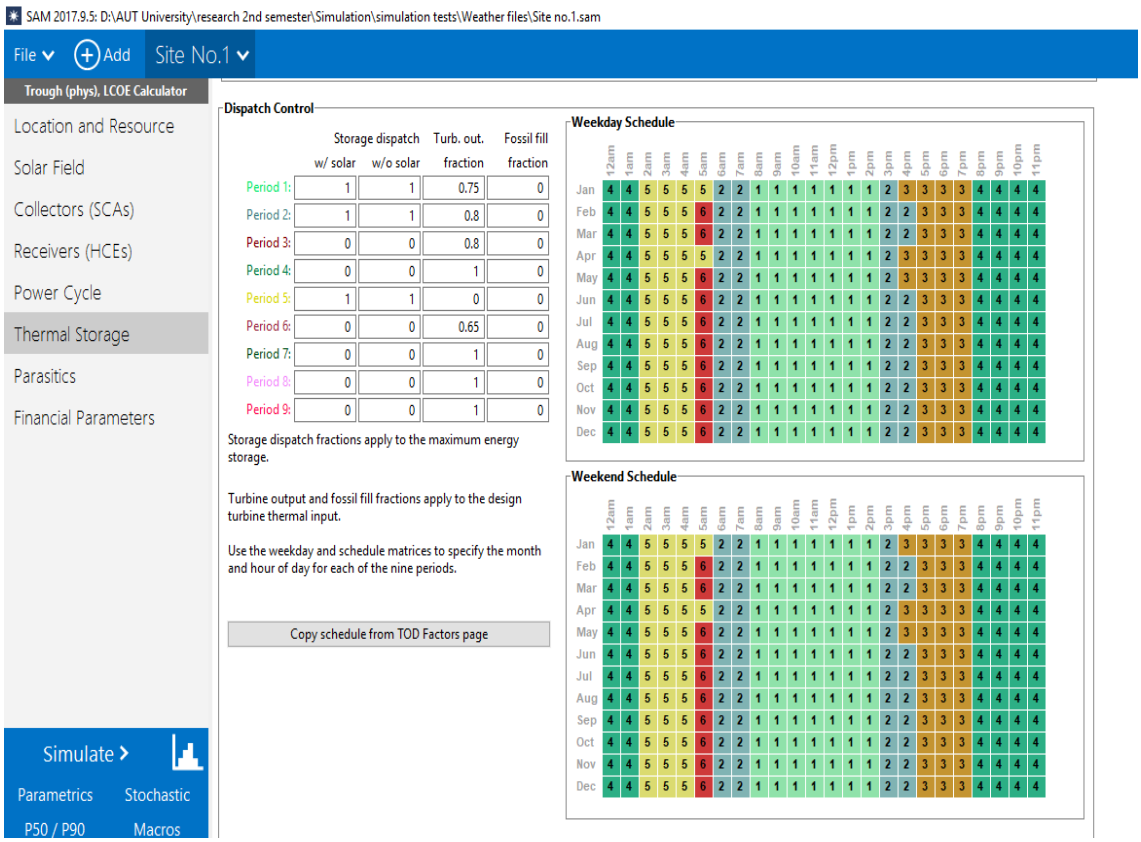

Figure (20): The dispatch control schedule of thermal storage.

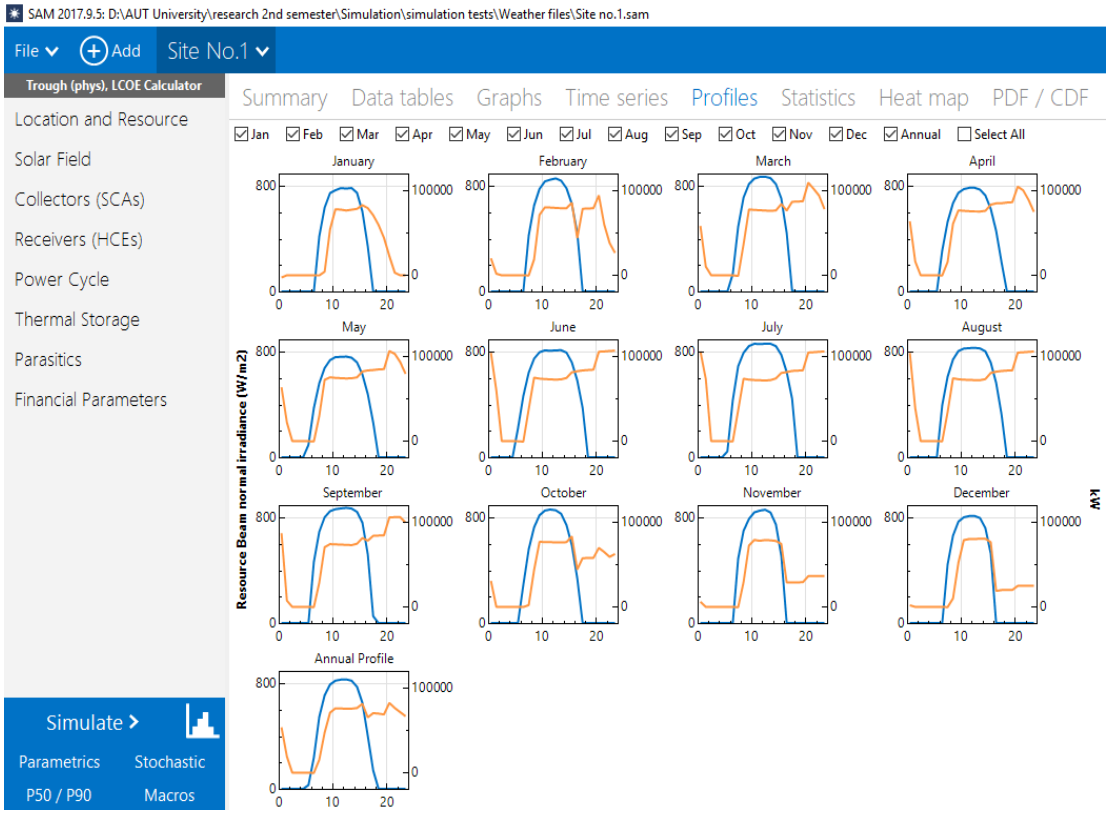

Figure (21): The monthly output of dispatch schedule compared to the monthly DNI during the day.

Table (10): The technical parameters used in SAM.

Technical parameters	Value
Solar multiple (actual)	2.5
Solar field area (km²)	2.877
Field aperture (km²)	1.1
Total land area (km²)	4
Row spacing (m)	15
Field subsection	6
Number of loops	253
Collector	Luz LS-3
Receiver	Siemens UVAC 2010
HTF	Therminol VP-1
Thermal storage (TES)	Therminol VP-1
Full load hours of TES	8

3.2 Financial Parameters According to the Egyptian Energy Market

After finalising the technical parameters, the second part of this study involved setting the values of the financial parameters. These values need to be set according to the current status of the Egyptian energy market. In setting these parameters, the following concepts need to be accounted for:

- Fixed charge rate: the amount of revenue required to cover the investment costs. This means the amount of revenue per dollar of investment that would be collected annually from customers to pay the carried charges on that investment, including return on equity and depreciation [61].
- Capital cost: the total investment cost of the project in dollars [31].
- Fixed operating cost: the fixed annual operating cost in dollars [31].
- Variable operating cost: The variable annual operating cost in dollars [31].
- Inflation rate: The total increase in the weighted average of prices for different goods [62].
- Internal rate of return: The project's annual nominal rate of return on equity requirement [31].

- Project term debt (DF): the size of debt represented as a percentage of the capital cost [31].
- Nominal debt interest rate (NINT): the nominal debt interest rate per annum.
- Effective tax rate: total income tax rate [31].
- Depreciation schedule: refers to the depreciation schedule per annum, based on the project's capital cost [31].
- Annual cost during construction: the construction cost per annum as a percentage of the capital cost [31].
- Nominal construction interest rate (CINT): the construction interest rate per annum on construction finance [31].

According to the Egyptian renewable energy market scenarios, which can be used in cases of large renewable energy power plants, there are two methods of competitive bidding to adopt such projects: for a state-owned power plant the project will be developed by NREA by using an Engineering, Procurement and Construction (EPC) model, while for a privately-owned power plant using a Build Own Operate (BOO) model, the investors will be responsible for building and operating the renewable energy power plant. Both scenarios are compatible with large CSP plants and both suggest a contracting period of 25 years in the case of solar energy [63], and thus that period was used for the analysis in this study.

In undertaking a long-term financial analysis, it is important to consider the inflation rate. The Egyptian economy at the time of writing (2018) is somewhat different to earlier years due to the drastic changes in the currency market after the floating of the Egyptian pound in 2016 [64]. Figure (22) shows the inflation rate over the past 25 years.

To have a realistic value that matches the current status of the Egyptian economy, an average value of the inflation rate over the past 25 years was assumed to be representative of inflation over the term of this analysis.

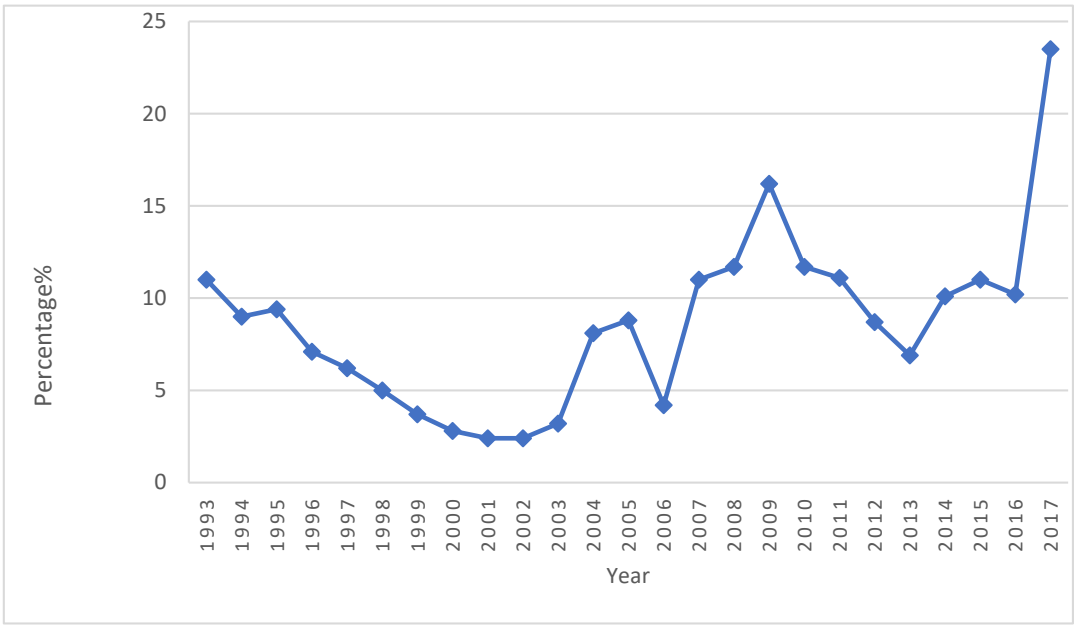

Figure (22): Inflation rate in Egypt for the past 25 years [62].

In their analysis, Hussein et al. [65] discussed the current and the possible future costs for renewable energy technologies in the Egyptian energy market which included a parabolic trough power plant of 100 MW with and without thermal storage. The values from this study for the parabolic trough plant with eight hours thermal storage were used in this research to provide a realistic benchmark. Some of the financial parameters that were based on [65] are the internal rate of return, which was set as 18% per year, the project term debt, set to 70% of the capital cost, and the nominal debt interest rate, which was set at 9.5% per annum.

For the capital cost value, also given in [65], there were two assumptions based on current installed power plants and external market studies: the first assumed capital cost in the case of low investment is 4600 US$/kW, and the second assumed investment is a maximum of 5850 US$/kW. An average of the two values was taken for this analysis. Two other inputs based on the above are assumed accordingly: the fixed operating cost was taken to be 22 US$/kW per annum, and the variable operating cost 0.02 US$/kW per annum.

The financial assumptions in the SAM also include the effective tax rate, set at 22.5% as in Egypt in 2015 the Ministry of Finance declared that the rate of the taxes for corporate profits for both foreigners and nationals would be reduced from the previous rate of 25% [66]. Given the proposed life time of the project was 25 years, the depreciation of the capital cost would be 4% per annum. Further, the annual cost during construction as a

percentage of the capital cost was set to 80% in the first year and 10% for both the second and third years. A nominal construction interest rate was assumed 9% as this value is affected by the inflation rate. Table (11) indicates the values that were used for the financial model in this study.

Table (11): The financial parameters used in the financial model.

Financial parameters	Value
Capital cost ($/kW)	5225
Fixed operating cost (annual) ($/kW)	22
Variable Operating cost ($/kWh)	0.02
Analysis period (years)	25
Inflation rate (%)	8.6
Internal rate of return (nominal) (%)	18
Project term debt (%)	70
Nominal debt interest rate (%)	9.5
Effective tax rate (%)	22.5
Depreciation schedule (%)	4
Nominal construction interest rate (%)	9

In performing the financial analysis, the SAM calculates the LCOE by using the fixed charge rate method. There are two options in doing this, either entering the fixed charge rate value itself or calculating it based on the previously mentioned values. The second method was followed; however, this approach depends on three factors. The first factor is the capital recovery factor (CRF), which is a function of the weighted average cost of the capital (WACC) as shown in equation (3 -1) [31]:

$$CRF = \frac{WACC}{1-\frac{1}{(1+WACC)^N}} \quad (3 - 1)$$

N is the analysis period in that case, and the WACC value can be obtained from equation (3 - 2):

$$WACC = \frac{1+(1-DF)\times((1+RROE)\times(1+i)-1))+DF\times((1+RINT)\times(1+i)-1)\times(1-TAX)}{1+i} \quad (3 - 2)$$

(i) is the inflation rate, PROE is the real return on investment, RINT is the real debt interest rate, and these two values are obtained from equations (3 - 3) and (3 - 4) [31]:

$$PROE = \frac{1+IRR}{1+i} - 1 \quad (3 - 3)$$

$$RINT = \frac{1+NINT}{1+i} - 1 \quad (3 - 4)$$

The second factor is the Project Financing Factor (PFF), which refers to the construction financing costs. This value is also calculated by the SAM from the construction cost schedule, effective tax rate (TAX) and depreciation schedule, as shown in equation (3 - 5) [31]:

$$PFF = \frac{1-(TAX \times PVDEP)}{1-TAX} \quad (3 - 5)$$

PVDEP in this case is the present value of depreciation, its value based on the depreciation and the WACC, as shown in equation (3 - 6) [31]:

$$PVDEP = \sum_{n=0}^{N} \frac{DEPn}{((1+WACC) \times (i+1)^{(n+1)}} \quad (3 - 6)$$

The third factor is the construction financing factor (CFF), which is a function of construction cost schedule, effective tax rate, and nominal construction financing interest rate, as shown in equation (3 -7) [31]:

$$CFF = \sum_{c=0}^{c} CON(c) \times (1 + (1 - TAX) \times ((1 + CINT)^{(c+0.5)} - 1)) \quad (3 - 7)$$

From the previous equations, the fixed charge rate value can be obtained from equation (3 - 8) [31]:

$$FCR = CRF \times PFF \times CFF \quad (3 - 8)$$

Finally, the LCOE can be calculated through equation (3 - 9) [31], [61]:

$$LCOE = \frac{FCR \times CC}{Q} + \frac{FOC}{Q} + VOC \quad (3 - 9)$$

CC is the capital cost, FOC is the fixed operating cost, VOC is the variable operating cost, and Q is the annual energy generated by the plant.

3.3 Results and Discussion

From the previous chapter, according to the siting study grading criteria, the first selected site had score of 91% and the second site had 88% while the third location had score of 80%. And after conducting the SAM simulation, the results showed the expected performance of the proposed CSP plant that matched the previous results, as the first site had the highest electrical generation output and lowest LCOE, followed by second and third sites respectively. These results also matched the DNI values for each selected site, as, at the first site, the daily DNI according to Meteonorm weather files was 7.58 kWh

/m^2/day followed by the second and third site with daily DNI of 7.05 kWh/m^2/day and 6.43 kWh/m^2/day respectively. Thus, it confirmed the appropriateness of the three selected locations and also gave assurance in the results obtained from the siting study.

The effect of the thermal storage used in this analysis can be clearly seen through the energy output shifting from daytime to evening hours as the peak load pattern was followed. The blue line in Figure (23) shows the hourly profile of the actual energy output of the first selected site, while the orange line represents the received DNI in this location.

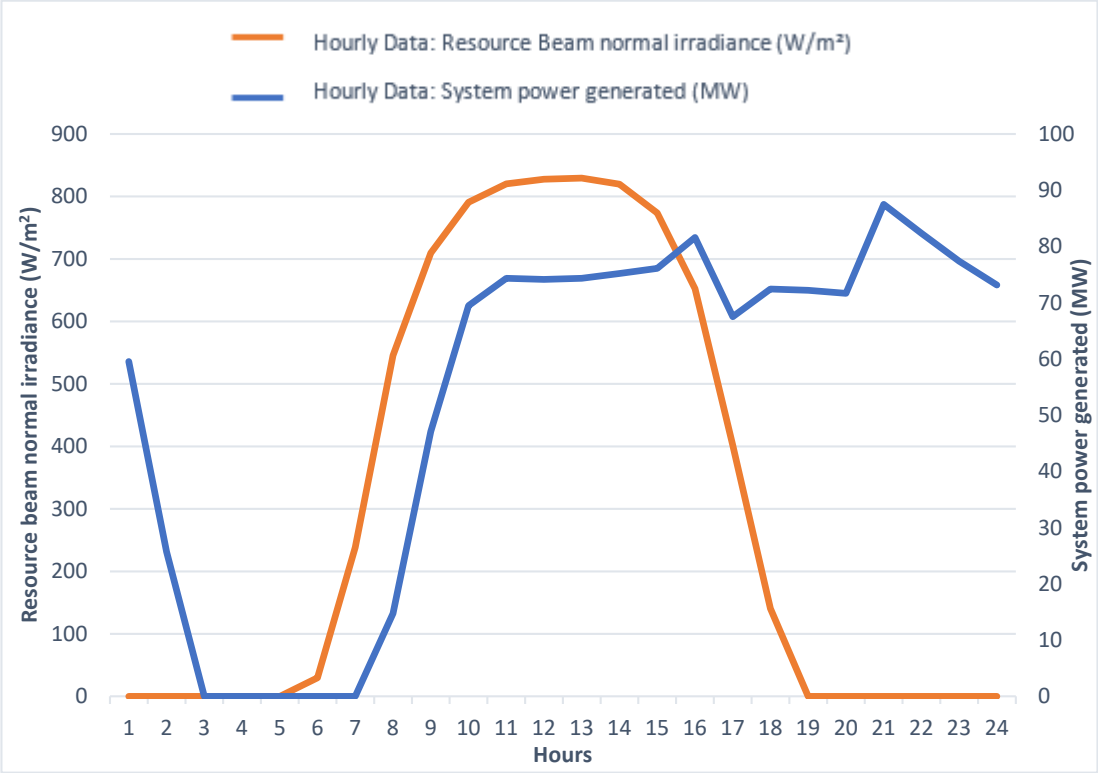

Figure (23): The hourly profile of the electrical energy output compared to the received DNI at the first site.

On the other hand, the annual thermal energy delivered to the power block and the annual thermal energy generated by the field for the three sites had the same order of value of generated energy. The biggest annual generation of thermal energy was the first site at around 1600 GWh, delivering around 1400 GWh. The second site came in second place, with a value close to site (1), while in third place, site (3) generated 1300 GWh of thermal energy from the field, with 1200 GWh of energy delivered to the power cycle.

As for the monthly electrical energy output from the three sites, shown in Figure (24), in the summer months the values are nearly equal, and during winter the energy produced in each month in both sites (1) and (2) are quite close, but still the third site had less energy produced per year compared to the other two sites.

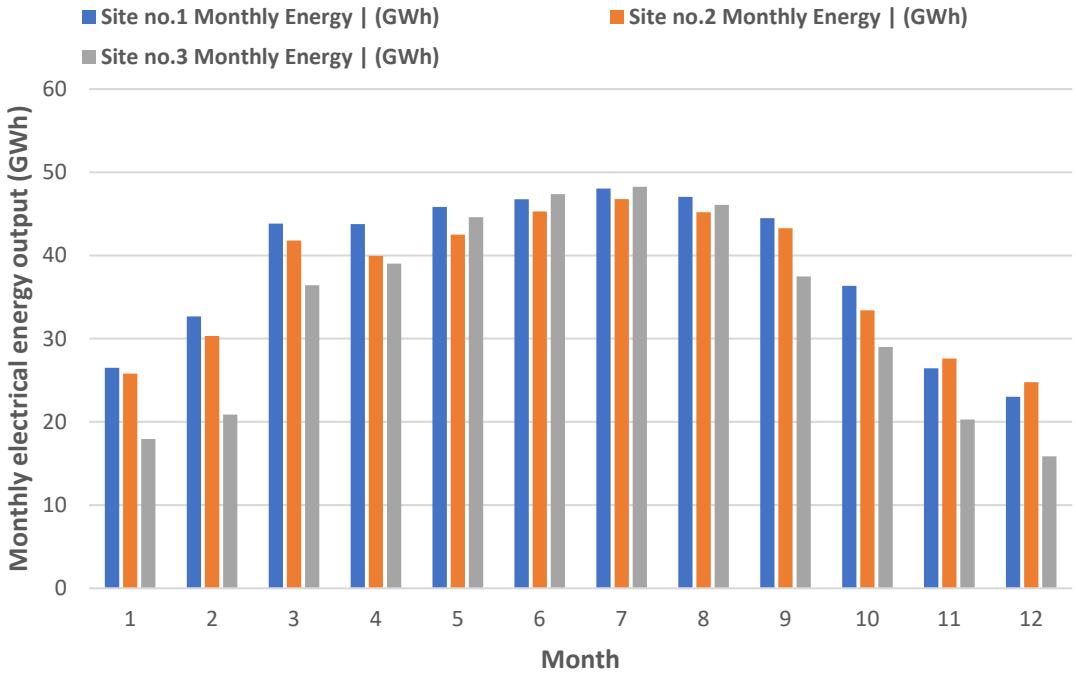

Figure (24): Monthly electrical energy output for the three selected sites.

The SAM analysis showed that the first selected site (28.06 N, 33.25 E) had the lowest LCOE at 10.07 US¢/kWh and it had the highest value of produced annual energy at 464.68 GWh and had the highest capacity factor at 53.1%. At the second selected site (27.27 N, 33.66 E), the LCOE was slightly higher at 10.4 US ¢/kWh. This site also delivered less annual energy, about 446.7 GWh, and had a lower capacity factor at 51.04 %. Finally, the third site (29.61 N, 32.75 E) had the highest LCOE 11.3 US ¢/kWh, the lowest energy production 403.14 GWh, and capacity factor 46.1 %. A summary of the results for the three sites is shown in Table (12).

Table (12): Summary of the outputs of each site.

Site	**Site (1)** **28.06 N, 33.25 E**	**Site (2)** **27.27 N, 33.66 E**	**Site (3)** **29.61 N, 32.75 E**
Annual energy (GWh)	464.68	446.7	403.14
Capacity factor (%)	53.1	51.04	46.07
Gross to Net Conversion Factor (%)	90.45	90.57	90.66
Electrical source - Power cycle gross output (GWh)	535.17	513.75	463.24
Thermal energy to the power block (GWh)	1445.15	1395.26	1255.91
Thermal power produced by the field (GWh)	1568.99	1473.73	1313.98
LCOE(¢/kWh)	10.07	10.4	11.30

Furthermore, a comparison was made between the results obtained from the SAM simulation model presented here and SAM models that were discussed earlier in Chapter 1, section 1.5, on related work and similar studies. The lowest levelised cost of energy among the three selected sites was found to be 10.07 US¢/kWh compared to the lowest LCOE in Algeria of 11.93 US¢/kWh in [32] and 34.55 US¢/kWh in [29], while the highest value of the capacity factor was found to be 53% in the present study, compared to around 40% in [32] with 6 hours of full load hours thermal storage and 43% in [29] with 8 hours of full load hours thermal storage. A detailed comparison of the present study, and [32] and [29] is shown in Table (13). Also, it is worth mentioning that in [41] the study also showed LCOE results ranging from 23 US¢/kWh to 23.4 US¢/kWh for Egypt.

Table (13): A comparison between [32] and [29] CSP models and the proposed model in the present study.

Study/Reference	**The proposed model**	**Abbas et al.** [32]	**Mihoub et al.** [29]
Capacity (MW)	100	100	50
Technology type	Parabolic trough	Parabolic trough	Parabolic trough
Full load hours of storage	8	6	8
Capacity factor (%)	46.1 - 53.1	21.1- 44.2	43.38 - 43.79
Storage fluid	Therminol VP-1	Solar salt	Therminol VP-1/ Molten salt
Solar multiple	2.5	2	3.1

All the previous assert the fact that CSP technology can be adopted on a bigger scale during the upcoming years of future energy plan. In addition, the electrical energy output from the SAM will be used in the next stage of modelling the power system model to ensure the grid integration performance.

3.4 Summary

In this chapter, the SAM was used to calculate the LCOE and the electrical energy output of the proposed CSP plant located at the three selected sites. Parabolic trough technology was selected to be used in the CSP SAM model. The system was designed to include thermal storage of eight full load hours. The technical parameters used in the SAM model were identified to achieve optimum performance while the financial parameters were set according to the Egyptian energy market status. It was found that the first selected site had the highest level of electrical energy output and lowest LCOE followed by the second and the third sites respectively. The hourly profile electrical output that was generated in this simulation is used in the next stage of this study.

Chapter 4 Power System Model

Having selected the best site for the proposed CSP plant, a power system model was designed using Simulink [67] to perform a load flow analysis of the system when integrated into the Egyptian national grid. The first selected site is located at 28.06 N, 33.25 E, which is near to both the 220 kV transmission lines and load centre, as shown in Figure (25). Based on the location, the proposed CSP plant is considered an additional power system to be integrated to an existing grid network. The proposed power system model is shown in Figure (26). This model included generation, transmission and load stages.

Figure (25): Map of the first selected site showing the transmission lines and load centre.

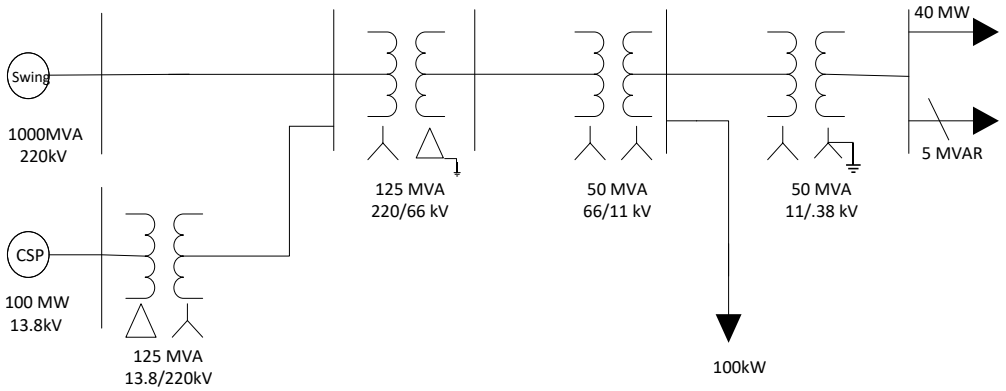

Figure (26): The single line diagram of the proposed power system model.

4.1 Power Flow Analysis

Conducting power flow studies is important to assure the performance of the proposed CSP plant in three ways. Firstly, it is important for estimating the losses of the proposed system. Secondly, it is important to determine the real and reactive power limits of the generation unit. Thirdly, it is important to ensure that the transmission lines and transformers are not overloaded or underloaded, and to calculate the bus voltage magnitudes and angles [68], [69].

The first step in power flow calculations is to obtain the input data which include: bus data, transmission line data, and transformer data. Each bus is associated with four variables: voltage magnitude, phase angle, net real power, and reactive power supplied to the bus. At each bus, two of these variables are known, and the other two must be computed by power flow calculations, whether manually or via suitable software [68].

4.1.1 Bus Classification

Before the load flow calculation is conducted, the types of the buses in power systems need to be clarified. A bus is a node at a line or many lines where one or many loads and generators are connected in a power network. In general buses are classified as follows:

- Load bus: A bus at which no generation exists, and only load is connected. The two known quantities for this bus are active load demand P_d and reactive load demand Q_d, hence it is usually defined as a P-Q bus. The other unknown quantities are the voltage magnitude and its phase angle. In this case, both quantities of real and reactive load demand are negative, since the generated power values P_g and Q_g always are assumed positive [68], [69].

- Voltage controlled bus: Also called a generator bus or P-V bus. At this bus, the voltage magnitude can be controlled. The real power in this case is generated by a synchronous generator which can be varied by changing the mechanical input; accordingly, the rotor axis position will change with respect to reference axis or reference bus, which means the phase angle of the rotor δ is directly related to the real power generated by the machine [69]. As for the voltage magnitude, it is governed by the excitation current in the field winding. Hence, at a generator bus, the real power generation P_g and voltage magnitude $|V_g|$ are known values, while the reactive power Q_g and phase angle δg are unknown and need to be computed [69].

- Slack bus: In any power network, the power flows from the generators to loads through transmission lines. Consequently, power losses occur in power conductors, which leads to the power balance equations (4 - 1) and (4 – 2) [69]:

$$P_g - P_d - P_L = 0 \quad (4 - 1)$$

$$Q_g - Q_d - Q_L = 0 \quad (4 - 2)$$

P_g and Q_g are the total real and reactive generations, P_d and Q_d are the total real and reactive power demands, and P_L and Q_L are the total power losses in transmission network [69].

The values of P_g, Q_g, P_d and Q_d are known or estimated, and the power losses P_L and Q_L are unknown and need to be calculated after the analysis of the power flow in the network [69]. Yet these losses have to be supplied by the generators of the system. For this reason, one of the generators or generating buses is identified as the slack bus or swing bus; at this bus both P_g and Q_g are not specified [69].

In addition, the voltage phase angle has a fixed value which is usually 0°, hence, all the voltage phase angles values are measured with respect to this bus which makes it the only reference bus in the system. All system losses are supplied by the generation at this bus [69].

4.2 Power System Model Parameters

4.2.1 Synchronous Generator

In performing the load flow analysis, the CSP system was modelled as a synchronous generator with a time varying input (based on the SAM generated output). The salient pole type PU fundamental synchronous machine was used in the Simulink model. There are two modes in which the machine in Simulink can be used, either as motor with a negative mechanical power (Pm) input or as a generator with a positive mechanical power (Pm) input; the other input is field voltage (Vf). In addition, there are three preferences for setting the mechanical input which can be by setting the value of the mechanical power manually, or through an excitation system, or by setting the rotation speed [67]. The method of setting the mechanical power input (Pm) value manually was used in the model proposed here. Other parameters of the selected synchronous machine included nominal power in VA, the r.m.s. voltage value, and the frequency in Hz.

In identifying the generator type either as a PV (power, voltage) generator or PQ (power, reactive power), the first option (PV) was selected for several reasons: firstly, the PQ type means that the reactive power will be set to a certain value which cannot be specified before the load flow is conducted. Secondly, the generator type also cannot be identified as a swing bus, as this means there will be no limits for both active and reactive power which cannot actually happen. In addition, the choice is made according to the assumption that the plant is not isolated from the whole grid network, which is the only case in which the generator can be set as a swing bus. Lastly, the value of the active power generation was set according to the hourly profile of electrical output generated from the SAM.

As for other parameter settings, starting with the nominal power, as stated in the third chapter the gross output from the proposed CSP plant is 111 MW, so the same value was used for the nominal power. As for the frequency, in Egypt the frequency is 50 Hz [70], consequently this value was used in the parameter settings. As for the voltage it was set at 13.8 kV, as the voltage ratings in large generators are usually between 10 and 15 kV. The field voltage was not determined at this stage so, for the synchronous generator, both inputs, the mechanical power and field voltage, were left at default values of 1 p.u. for each by using constant parameter input.

4.2.2 **Three-Phase Transformers**

Three-phase transformers (two windings) were included in the proposed model. After generating the power from the generation unit, and after checking the ratings of the transmission lines that were located near the selected sites, it was found that most of them were near to 220 kV lines. Also, one of the selected sites was close to both 500 and 220 kV lines. Consequently, power transformers had to be included in the power system model to level up the voltage rating to the required voltage level or for stepping down the voltage rating.

In the proposed model, one step-up transformer and three step-down transformers and a grounding transformer were included. The configuration for the connections of the first three-phase step-up transformer was a Delta-Star connection. As in this case it would be used as step-up transformer, this connection has many advantages. On the primary side, the cross-section required will be smaller and, as the secondary side is star connected, that means there is a neutral available which can be used for a three-phase four-wire system [71]. The step-up transformer MVA rating is 125 MVA, the voltages for the primary and

secondary windings are 13.8 and 220 kV respectively. All the transformers' parameters that were used in the power system model are shown in Table (14).

The second transformer is a step-down transformer, from 220 kV to 66 kV, with a rating of 125 MVA. The connection type is a Star-Delta connection. This connection method is usually recommended for large high voltage step-down transformers as it will be more economical as the number of turns required for the primary side would be less [72].

As for the third transformer, a grounding transformer was added to the model, as in any distribution system, a grounding transformer is always needed, for several reasons. Firstly, occasionally it is used to convert a three-wire ungrounded circuit to a four-wire grounded circuit. Secondly, the grounding transformer handles the unbalanced load on the circuit. Thirdly, it is used where utilities need a ground source during abnormal conditions. A zigzag grounding bank was used for its high efficiency [73]. The transformer power and frequency ratings were 100 MW and 50 Hz respectively.

The last two transformers that were used were a step-down transformer from 66 to 11 kV, and a step-down transformer from 11 kV to 380 V. These ratings were selected based on the voltage ratings used in power transmission networks in Egypt [74]. The first of these transformers had a Star-Star connection, as this connection is usually used in substations as no phase angle displacements can happen in Star-Star connection [75]. As for the last distribution transformer, it had Star-Star grounded neutral connection as the distribution transformer used in substations is usually grounded for safety reasons and the system should be grounded from at least one side of the two windings.

Table (14): Ratings for the three-phase transformers that are used in the proposed power system model.

Transformer No.	Primary Winding Voltage (kV)	Secondary Winding Voltage (kV)	MVA Ratings*	Frequency (Hz)	Configuration
1	13.8	220	125	50	Delta/Star
2	220	66	125	50	Star/Delta
3	66	11	50	50	Star/Star
4	11	0.38	50	50	Star/Grounded Star
5 (grounding transformer)	66		100	50	Zig Zag

*The MVA ratings used in the power system model were decided based on the power transformers that have been used in the Egyptian grid network, which were supplied by a local company manufacturing transformers and other electrical products [76].

4.2.3 **Three-Phase Transmission Line**

To transport the power generated from the power plant, grid integration will be needed, thus a connection with the nearest transmission line network is necessary. The transmission line model has three types according to its length. Firstly, short transmission lines have a length of less than 80 km, and in this case the equivalent circuit of the line could be represented as a series resistance and inductive reactance [68], [77]. Secondly, medium transmission lines are between 80 km and 240 km in length, and in this equivalent circuit, the capacitance is represented in the circuit shunt connected and divided into two equal parts, each placed at the sending and receiving ends of the line which can be a π or T section line [68], [77]. Table (15) shows comparison between each type.

Thirdly, the last type, which are long distance transmission lines, the line length in this type is more than 240 km. Usually in this type the equivalent circuit is represented as a distributed parameter line which includes resistance, inductance and capacitance uniformly distributed along the line, or the π section line still can be used for lengths up to 300 km only [68], [77].

The distance between the proposed plant and the nearest transmission line is 1 km only, while the distance from the transmission line to the load centre was considered to be 5 km, as at the first selected site. Consequently, this distance was used in the model as a part of the transmission line transporting from the 220 kV transmission line to the step-down transformer of 220/66 kV as the 1 km distance was neglected between the station and the 220 kV network. Thus, in this power system model a three-phase series resistance, inductance, conductance (RLC) branch was used as a representation of a three-phase transmission line.

As the short-line model was used, the capacitance was neglected, hence, the equivalent circuit included only series resistance and inductive reactance. The resistance could be calculated by using equation (4 - 3) [68]:

$$R = \rho \frac{l}{a} \qquad (4 - 3)$$

where R is the resistance of the conductor, l is the length, a is the cross-sectional area and ρ is the resistivity of the conductor.

Table (15): Comparison between transmission line models [68], [78], [79].

Transmission line (T.L.) model	**Short T.L. Model**	**Medium T.L. Model**		**Long T.L. Model**
		T Section	**Π Section**	
Distance (km)	Less than 80	80-240		More than 240
Equivalent circuit	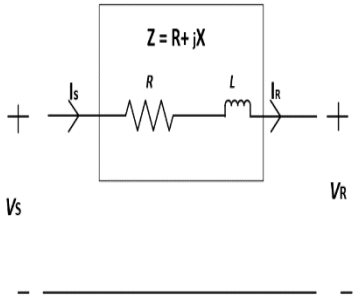	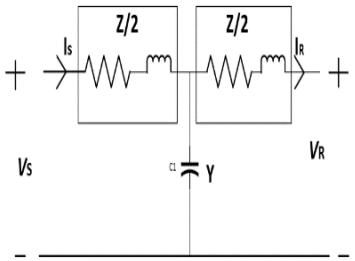	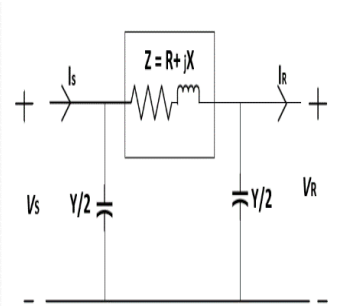	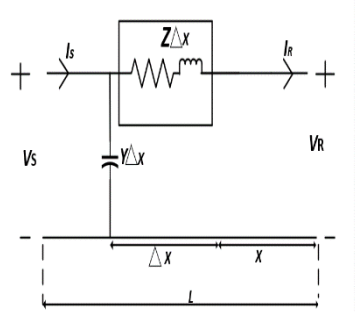
Comments	The capacitive effect is negligible, only resistance and inductive reactance are considered in the model	In T section model the impedance is divided into two equal parts, and they are placed on each side of the shunt capacitance.	In Π model, the shunt capacitance is divided into two equal parts, these parts are placed on the sending and receiving end of the transmission line.	In the distributed long-line model, the parameters are distributed uniformly, the corresponding impedance and capacitance are obtained by solving differential equations.

The resistivity is usually a constant based on the selected material, which is commonly Aluminium Conductor Steel Reinforced (ACSR), which is used for most overhead transmission lines and this kind of cable is also used in the Egyptian grid network [80]. In this model for calculating the value of the resistance the following points were considered:

- ACSR is the type of conductor material that is used in Egyptian transmission network specifically in this area (near to the Suez gulf region).
- According to the data sheet of a wind power development project [80], the 220 kV transmission lines in the Egyptian network that are currently used at the proposed sites are ACSR 380/50; these numbers represent the percentage of overall cross-section to steel reinforcement area.
- The technical specifications of similar types of conductors' material were found in the Electrical Research Standard Institute Reference Book for 220 kV and above [81]. Also, conductors with similar features produced by different companies were investigated [82]-[84]. It was found that the resistance for a quite similar type of material is around 0.075 Ω/km/phase (assuming each phase in the three-phase transmission line is represented in one conductor).
- As the distance from the proposed CSP plant and load centre was assumed to be 5 km, the calculated resistance was estimated as 1.125 Ω, according to equation (4 - 4):

$$R = r\ (\Omega/km/phase) \times 5\ (\text{No. of kilometres}) \times 3\ (\text{No. of phases}) \qquad (4 - 4)$$

After estimating the value of series resistance in the short transmission line model, next step was calculating the series inductive reactance (XL). This value represents both internal and external inductances due to conductors' internal and external flux [9]. The inductance of a transmission line is defined as the number of flux linkages produced per ampere of current flowing through the line [85]. In the case of a three-phase transmission line, the inductance (L) value was calculated based on the following:

- An average value was used for overall inductive reactance (XL) for a 220 kV transmission line, which was found to be around 0.4 Ω/km/phase [85], [86].
- In the Simulink model, a series resistance and reactance were used as a transmission line model, also the capacitance was neglected as mentioned before.

The parameters are R in Ω and L in H, and since the average value is expressed in Ω/km/phase, to convert the value, equation (4 - 5) was used [68], [79]:

$$XL = 2 \times \pi \times f \times L \qquad (4 - 5)$$

where f is the frequency, which in this case equals 50 Hz. Consequently, the value of L was found to be 1.27×10^{-3}H/km/phase.

- The total inductance of the three-phase line was found to be 0.01905 H, according to equation (4 - 6):

  L = L (H/km/phase) × 5 (No. of kilometres) × 3 (No. of phases) (4 - 6)

4.2.4 Three-Phase Loads

The next part that was included in the power system model was three-phase loads. The electric load is the part of the electric circuit that consumes power whether it is active or reactive power. The load type can be classified into three types, resistive, inductive, capacitive loads or some combination of the three. The first type consumes active power which is measured in watts; some examples of resistive loads are lightbulbs, toasters, and electric hot water heaters [87].

As for the inductive load, this kind of load requires a magnetic field to operate which will make the current lag the applied voltage; this is the reason for the consumption of reactive power which is measured in VARS. Examples of this type of load are hair dryers, fans, blenders, vacuum cleaners, and many other motorized devices, as all motors are inductive loads [87]. The last type, capacitive loads, are related to the devices that have capacitors in them, for instance, components used in electronic devices [87].

On the other hand, the electric load on power systems is classified according to the type of consumer. As an illustration, domestic (residential) loads, which include home appliances such as lights, fans, and refrigerators, usually occur for some hours during the day. In addition, there are commercial loads, such as shops and restaurants, which occur for a longer time during the day and continue into the night. Another type is the industrial load, which is related to load demand from industries and which ranges between 25 and 500 kW depending on the size of the industry itself [88]. The other types are irrigation loads, traction loads, and the load represented by street lights and water supply.

As information regarding the load demand in the selected locations was not available, instead, in the model, the load was set according the power output generated by the proposed CSP plant.

The average annual load cycle that was produced by the SAM, as shown in Table (16), was used to calculate the energy produced per day. As each value is the number of megawatts generated for one hour, consequently for the whole day the final value of the generated energy was 1276.3673 MWh/day. As a result, the average load in megawatts was calculated to be 53.18MW according to equation (4 - 7) [88]:

$$\text{Average load} = \frac{Generated\ Energy}{No.of\ hours} \tag{4 - 7}$$

The three-phase load that was added to the Simulink model should be less than the result obtained in the previous step, as that result will be considered as a maximum demand. Also, the load should be less than maximum limit between 15 to 20% of the generation [88]. In addition, in load flow, the load should be constant in order to perform load flow studies, as explained before in the power flow analysis section. Thus, a 45 MW three-phase load was used in the power system model. As mentioned, there was no information available regarding the actual grid data in this location. Hence, the load was set as 40 MW and 5 MVAR, to conduct the load flow simulation in case of both active and reactive load. The 45 MW load was connected in series at the receiving end.

There were two other loads used in the model. A load was used between the synchronous generator and the step-up transformer as they cannot be connected in series in the presence of the inductive element. A high resistive value needs to be connected with one of them, and a 100 kW parallel resistive load was used for this purpose [67]. In addition, another 100 kW load was used at the11 kV rating as an industrial load in the power system model.

Table (16): The hourly average of the annual profile of MW power generated during the day.

Time of day (Hours)	Hourly power generated (MW)	Time of day (Hours)	Hourly power generated (MW)
1	59.5413	13	74.336
2	25.7227	14	75.1951
3	0	15	76.091
4	0	16	81.5889
5	0	17	67.5139
6	0	18	72.4216
7	0	19	72.1877
8	14.7345	20	71.6728
9	47.0986	21	87.476
10	69.4682	22	82.3323
11	74.3236	23	77.3938
12	74.1426	24	73.1267

4.3 Load Flow Solution in Simulink

As stated in the bus classification, a swing bus is an essential part in the model if the system is not isolated, as represented in this case. For this reason, a swing bus was added to the model to provide the losses of the transmission network. This swing bus was set at 1000 MVA with a base voltage of 220 kV that matched with the transmission network voltage; its voltage phase angle was 0° as this bus was the reference for all the buses in the model. Simulink provides load flow buses that can be used in this model as bus identification for each stage of transmission. Six of them were added to the model, one at 13.8 kV generation after the synchronous generator, also one by the swing bus with 220 kV and after the 220 kV transmission stage, in addition buses were added at 66 kV, 11 kV and 0.38 kV loads. The load buses' input data are shown in Table (17); for the detailed Simulink model see Appendix B.

Table (17): Bus input data.

Bus type	**Bus No.**	**V Base (kV)**	**V ref (P.U.)**	**Phase angle (deg)**	**P (MW)**	**Q (MVAR)**
PV	1	13.8	1	-	100	-
Swing	2	220	1	0	-	-
Load	3	220	-	-	0	0
Load	4	66	-	-	0	0
Load	5	11	-	-	0.1	0
Load	6	0.38	-	-	40	5

4.4 Results and Discussion

After conducting the load flow simulation for every hour of generation during the day, it was noticed that during the first hour of generation of the CSP plant with 59 MW approximated generated power, the losses in the same time period were around 0.4 MW and 14 MVAR. The phase angle at 13.8 KV bus was -25.65°, furthermore the simulation provided the mechanical power value, and the field voltages which were 0.53 p.u. and 1.15 p.u. of stator voltage. During the period when the generation power was highest, at 87 MW, the loss values were the highest, reaching 0.56 MW and 19.65 MVAR; this matched the hour of the peak at 9 pm. On the other hand, there were five hours of non-generation of power (zero MW) from 2am to 7 am. Finally, during the last hour of day,

the CSP plant generated around 73 MW and the total system losses were 0.49 MW and 16.7 MVAR with 0.66 p.u. mechanical power and 1.23 p.u. of field voltage. A selection of the results of the load flow solution is shown in Table (18); for the detailed results see Appendix B. As stated before in relation to the importance of a swing bus in load flow calculations, it was clear that it was responsible for providing system losses, especially as the reactive power is always needed for transmitting the power with all the losses included. Also, due to the short distance to load centres, the power losses were less.

In addition, when the CSP was not generating the required power, the swing bus provided this power as the loads are constant, they will always need to be met. Also, it was noticed that all the buses followed the reference bus, which in this case is the swing bus. Consequently, the p.u. voltage values and phase angles in the 66 kV, 11 kV and 0.38 kV buses were not changed during the whole day of simulation, which confirmed the system reliability. As for the 13.8 KV bus, the phase angle changed through the day, according to the changing field voltage and mechanical power input each time in the synchronous generator.

At each time in the simulation, the value of both mechanical power and field voltage were obtained, an Excel file was created for each value and these values were used as input for the synchronous generator (mechanical power and field voltage) to show the output for 24 hours. As shown in Figure (27), the daily output power for the synchronous generator (CSP plant representation) matches the non-generating hours' output as, in this case, the active power output was zero between 2am and 7 am; also the reactive power values during the 24 hours matched the load flow results.

Table (18): Selection of the results obtained from the load flow solution in Simulink.

Hours	Total Generation	Total PQ load	Total losses	Swing bus P & Q	CSP P &Q	Voltage (p.u.) and angle (deg)					No. of iterations	P mechanical (p.u.)*	Vf (p.u.)*
						Bus 13.8	Bus 220	Bus 66	Bus11 (load)	Bus 380 (load)			
1	41.55 MW/ 20.18 Mvar	40.20 MW/ 5.00 Mvar	0.43 MW/ 14.40 Mvar	-18.04 MW/ 19.28 Mvar	59.54 MW/ 0.90 Mvar	1/ -25.65°	1/ 0°	0.982/ -32.54°	0.946/ -40.48°	0.938/ -43.06°	2	0.54	1.15
2	41.41 MW/ 16.51 Mvar	40.20 MW/ 5.00 Mvar	0.34 MW/ 18.25 Mvar	15.68 MW/ 16.60 Mvar	25.72 MW/ 0 Mvar	1/ -28.13°	1/ 0°	0.982/ -32.54°	0.946/ -40.48°	0.938/ -43.06°	2	0.23	1.03
21	41.63 MW/ 25.43 Mvar	40.20 MW/ 5.00 Mvar	0.56 MW/ 19.65 Mvar	-45.85 MW/ 22.60 Mvar	87.48 MW/ 2.83 Mvar	1/ -23.59°	1/ 0°	0.982/ -32.54°	0.946/ -40.48°	0.938/ -43.06°	2	0.79	1.33
24	41.55 MW/ 22.48 Mvar	40.20 MW/ 5.00 Mvar	0.49 MW/ 16.70 Mvar	-31.57 MW/ 20.77 Mvar	73.13 MW/ 1.71 Mvar	1/ -24.65°	1/ 0°	0.982/ -32.54°	0.946/ -40.48°	0.938/ -43.06°	2	0.66	1.23

*Both the field voltage and the mechanical power input values were obtained during the load flow analysis assuming the value of the active output power based on SAM results in the previous chapter.

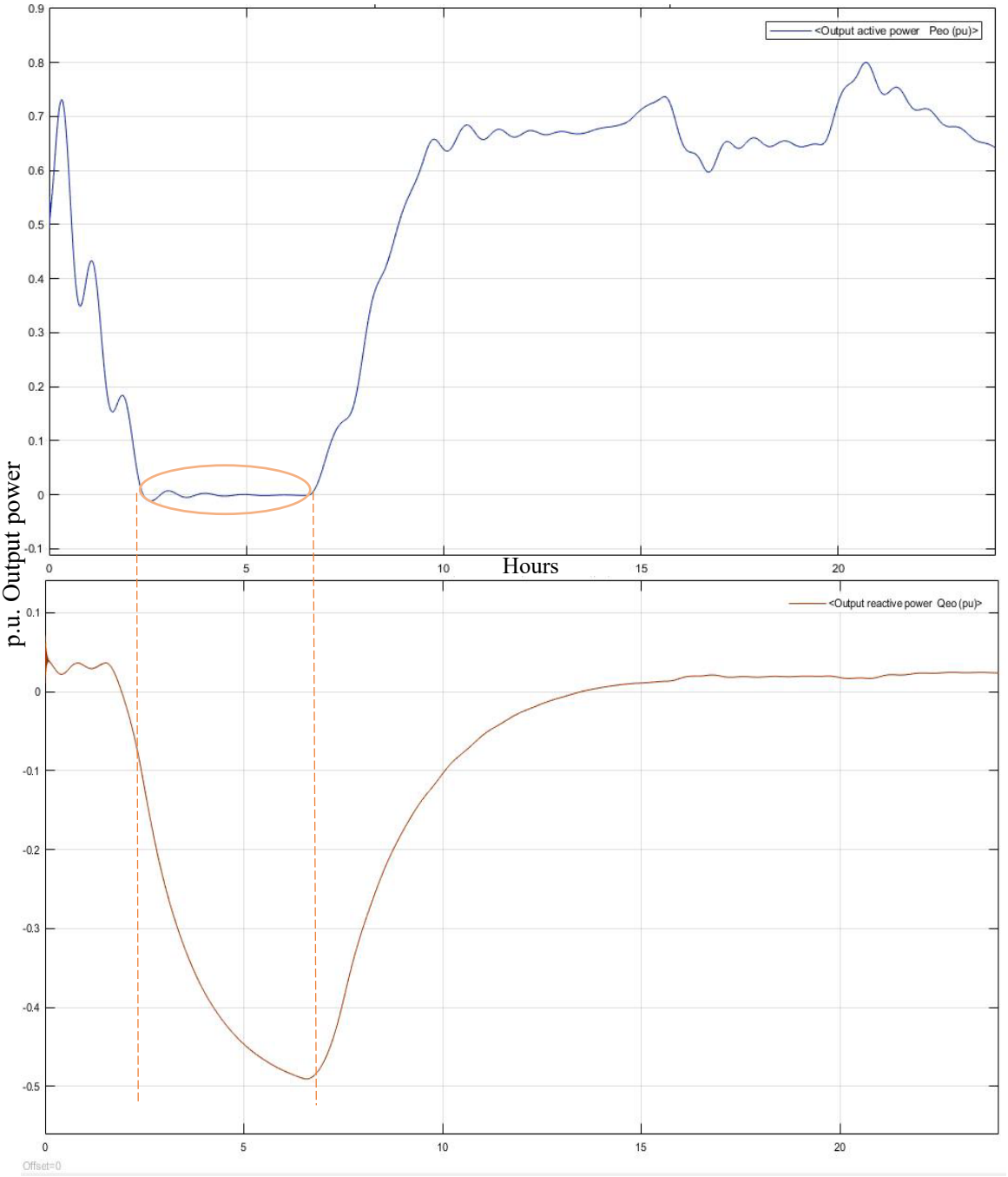

Figure (27): The active and reactive power generated for 24 hours including the non-generating hours.

This part of the research was conducted to investigate the grid integration of the proposed CSP plant and to carry out power flow studies. The study proved the compatibility of the system with the grid. In addition, it showed in the case of the non-generating hours, that the slack bus provided the losses which will occur for real if the CSP plant was integrated to the grid as it would not be the main source of power. Furthermore, as mentioned before, there was only one previous study, by Patel et al. [37], that combined modelling a CSP plant by MATLAB with grid integration, but in that research power flow studies were not conducted. The results showed a complete model of CSP plant with grid integration with a 22 kV voltage level, which was a different approach from the present study. A detailed comparison between [37] and the present study is shown in Table (19). Thus, the load flow study described here succeeded in presenting a different perspective in combining both SAM modelling and grid integration Simulink modelling, and performing power flow studies and giving a clearer image of the predicted performance of the proposed CSP plant when connected to the grid.

Table (19): Comparison between the present study and Patel et al. [37].

Study /Ref.	The present study	Patel et al. [37]
Simulink Model	Based on linking two software products together by using the output from SAM as an input for Simulink model.	Adapted from PV system model altered with some modifications to represent the components of CSP plant.
Power flow studies	Conducted by powergui tool in Simulink.	Not conducted.
Integration voltage level (KV)	220	22
Results	The simulation showed the values of active and reactive power, also, p.u. voltage and angle for each hour of the 24 hours of generation.	Grid interconnection with 22 KV voltage level with no load flow studies.

4.5 Summary

This chapter presented a power system model that was designed based on the Egyptian national grid voltage levels. A synchronous generator was used as a representation of the CSP plant and the hourly profile that was generated from the SAM was used as an input for the power system model. As the system was integrated to the grid, a slack bus was used to provide the power losses of the model. Simulink was used to conduct power load flow studies. Furthermore, the values of the p.u. voltage and phase angles of the buses were obtained, along with the values of the mechanical power input and field voltage of the generation unit for the 24-hour profile. In addition, an Excel file was created to be used as an input for the synchronous generator to show the predicted power output for 24 hours. The power system model designed in this research successfully presented the expected outcome from integrating the proposed CSP plant into the grid.

Chapter 5 Conclusion and Future Work

5.1 Conclusion

This thesis reports a study to assess CSP technology for Egyptian locations. The first stage was investigating the factors that affect the selection of possible locations for CSP plants. These factors were solar direct irradiance, land resources, the infrastructure of the national electrical grid, and access to the road network. A scan of all Egyptian locations was carried out using Google Maps and by comparing the maps of every relevant resource. Seven potential sites were selected, although these possible sites needed to be reduced to only three locations for detailed case studies.

Consequently, the previously mentioned factors were evaluated by using a multi-criteria analysis approach by using a weighing scale for each factor of 100%. DNI represented 50%; the distance to the nearest transmission line, the distance to the load centre, the distance to a water source were each given a score of 15%; and the final factor was the advantage of having a nearby renewable energy site, which scored 5%. Every factor individually was given a grade out of 10. As a result, three sites were selected for the next stage, these locations were located in eastern Egypt by the Red Sea, in particular on the Suez gulf.

The second stage started with the selection of the parabolic trough as a technology type for SAM simulation. Then both technical and economic parameters were set according to current economic status and the required performance. The results showed the lowest LCOE was found to be 10.07 US¢/kWh, with the best generation performance of an annual energy output of 464.7 GWh, which can be achieved at the first site located at 27.7˚ N and 33.7˚ E precisely.

The final stage was to design a power system model to assure grid integration. This model consisted of synchronous generator, transmission line and stepping up and stepping down transformers, and three phase loads. The output power data generated from the previous stage were exported to an Excel file with 24 values covering the full day. These values were used as an input for the active power tab in the synchronous generator to follow the same pattern of generation. Power flow studies were conducted and obtained the values of the p.u. voltages and voltage angle for each hour in addition to the active and reactive power. Also, the field voltage and mechanical power input values for the synchronous

generator were obtained, and a 24-hour simulation was conducted by Simulink for active and reactive power values.

Based on these case studies and results, installing CSP plants in Egypt can be seriously considered in the future. The results have shown a clear picture of all the stages that are observed before installing any CSP plant; furthermore, the power flow studies succeeded in presenting a vision of grid integration performance in such cases. The results clearly showed that CSP technology can be adopted on a bigger scale in Egypt and showed the locations that are suitable for a CSP installation, even with the current economic status of the country. Moreover, the study recommends altering some government financial policies that are related to investment in the power sector, to encourage this type of technology as a main part of Egypt's future energy plan.

5.2 Future Work

In future research, more data sources need to be accessed to have a better siting approach by using GIS software to compare between different resources to be assessed. Also, consideration should be given to investigating more western desert areas for potential locations, but this will require more information about the current actual status of such locations. In addition, future research should perform simulations with other CSP technologies in order to compare and analyse the performance of the different technologies, and evaluate the economic side based on the predicted economic status of the country. As for the grid integration studies, a more complex model needs to be designed that matches the current national grid connections in the selected places with more data on substations rating. Moreover, the load demand needs to be calculated depending on the actual status of the location's grid network and the real power factor in the selected area which will allow a precise power flow studies. In addition, investigating the power quality would be needed to decrease the losses that were found in the load flow solution.

References

[1] *Solar energy in Egypt* (n.d.) [Online]. Available: www.solartecegypt.com

[2] *Egypt's renewable energy country* (n.d.) [Online]. Available: http://www.rcreee.org

[3] *Concentrating solar power basics* (n.d.) [Online]. Available: https://www.energy.gov/eere/solar/articles/concentrating-solar-power-basics

[4] *Power tower system concentrating solar power basics* (n.d.) [Online]. Available: https://www.energy.gov/eere/solar/articles/power-tower-system-concentrating-solar-power-basics

[5] *Planta Solar 10* (n.d.) [Online]. Available: https://www.nrel.gov/csp/solarpaces/project_detail.cfm/projectID=38

[6] *Gemasolar thermosolar plant* (n.d.) [Online]. Available: https://www.nrel.gov/csp/solarpaces/project_detail.cfm/projectID=40

[7] C. Philibert, P. Frankl, and Z. Dobrotkova, "Technology Roadmap : Concentrating Solar Power," in *Technology Roadmap Report.* Paris, France: International Energy Agency, 2010.

[8] *Concentrating solar power projects by technology* (n.d.) [Online]. Available: https://www.nrel.gov/csp/solarpaces/by_technology.cfm

[9] H. Müller-Steinhagen and F. Trieb, "Concentrating solar power: A review of the technology," *Ingenia Inform QR Acad Eng,* vol. 18, pp. 43-50, 2004.

[10] I. Llorente García, J. L. Álvarez, and D. Blanco, "Performance model for parabolic trough solar thermal power plants with thermal storage: Comparison to operating plant data," *Solar Energy,* vol. 85, no. 10, pp. 2443-2460, 2011.

[11] H. Zhang, J. Baeyens, J. Degrève, and G. Cacères, "Concentrated solar power plants: Review and design methodology," *Renewable and Sustainable Energy Reviews,* vol. 22, pp. 466-481, 2013.

[12] F. Orioli and V. Orioli. (2009, May). *Parabolic or Fresnel?* [Online]. Available: http://www.soltigua.com/

[13] H. Hashem. (2012, Sept. 3). *Can Fresnel outperform parabolic trough?* [Online]. Available: http://analysis.newenergyupdate.com/csp-today/technology/can-fresnel-outperform-parabolic-trough

[14] *PE 1 in Spain* (n.d.) [Online]. Available: http://www.novatecsolar.com/49-1-PE-1.html

[15] D. Woernle. (2014, May). *Solar: Areva commissions molten salt energy storage demonstration* [Online]. Available: http://us.areva.com/EN/home-2970/areva-inc-areva-commissions-molten-salt-energy-storage-demonstration.html

[16] M. Moser, F. Trieb, and T. Fichter, "Potential of concentrating solar power plants for the combined production of water and electricity in MENA countries," *Journal of Sustainable Development of Energy, Water and Environment Systems,* vol. 1, no. 2, pp. 122-140, 2013.

[17] *Solar collector* (n.d.) [Online]. Available: http://energyeducation.ca/encyclopedia/Solar_collector#cite_ref-boyle_2-0

[18] G. Boyle, *Renewable Energy: Power for a Sustainable Future*, 2nd ed. Oxford, UK: Oxford University Press, 2004.

[19] *The solar receiver* (n.d.) [Online]. Available: http://energy.kth.se/compedu/webcompedu/webhelp/S9_Renewable_Energy/B5_Solar_Energy/C3_Advanced_Solar_Thermal/ID107_files/The_Solar_Receiver.htm

[20] J. Pacio and T. Wetzel, "Assessment of liquid metal technology status and research paths for their use as efficient heat transfer fluids in solar central receiver systems," *Solar Energy,* vol. 93, pp. 11-22, 2013.

[21] Y. Tian and C.-Y. Zhao, "A review of solar collectors and thermal energy storage in solar thermal applications," *Applied Energy,* vol. 104, pp. 538-553, 2013.

[22] K. Vignarooban, X. Xu, A. Arvay, K. Hsu, and A. Kannan, "Heat transfer fluids for concentrating solar power systems – A review," *Applied Energy,* vol. 146, pp. 383-396, 2015.

[23] X. Xu, K. Vignarooban, B. Xu, K. Hsu, and A. Kannan, "Prospects and problems of concentrating solar power technologies for power generation in the desert regions," *Renewable and Sustainable Energy Reviews,* vol. 53, pp. 1106-1131, 2016.

[24] J. G. Cordaro, N. C. Rubin, and R. W. Bradshaw, "Multicomponent molten salt mixtures based on nitrate/nitrite anions," *Journal of Solar Energy Engineering,* vol. 133, no. 1, 2011.

[25] T. Bauer, D. Laing, and R. Tamme, "Recent progress in alkali nitrate/nitrite developments for solar thermal power applications," in *Molten Salts Chemistry and Technology,* M. Gaune-Escard and G.M. Haarberg, Eds. Indianapolis, IN: Wiley, 2014, pp. 543-553.

[26] A. C. Köberle, D. E. Gernaat, and D. P. van Vuuren, "Assessing current and future techno-economic potential of concentrated solar power and photovoltaic electricity generation," *Energy,* vol. 89, pp. 739-756, 2015.

[27] M. J. Wagner and P. Gilman, *Technical Manual for the SAM Physical Trough Model*. National Renewable Energy Laboratory, Golden, CO, 2011.

[28] *Huanghe Qinghai Delingha solar thermal power project* (n.d.) [Online]. Available: https://www.power-technology.com/projects/huanghe-qinghai-delingha-solar-thermal-power-project/

[29] S. Mihoub, A. Chermiti and H. Beltagy, "Methodology of determining the optimum performances of future concentrating solar thermal power plants in Algeria" *Energy,* vol. 122, pp. 801-810, 2016.

[30] W. Short, D. J. Packey, and T. Holt, *A Manual for the Economic Evaluation of Energy Efficiency and Renewable Energy Technologies*. National Renewable Energy Laboratory, Golden, CO, 1995.

[31] *System Advisor Model, Version 2017.9.5 (SAM 2017.9.5)*. National Renewable Energy Laboratory, Golden, CO, 2017.

[32] M. Abbas, Z. Belgroun, H. Aburidah, and N. K. Merzouk, "Assessment of a solar parabolic trough power plant for electricity generation under Mediterranean and arid climate conditions in Algeria," *Energy Procedia,* vol. 42, pp. 93-102, 2013.

[33] I. Purohit and P. Purohit, "Technical and economic potential of concentrating solar thermal power generation in India," *Renewable and Sustainable Energy Reviews,* vol. 78, pp. 648-667, 2017.

[34] M. S. Al-Soud and E. S. Hrayshat, "A 50 MW concentrating solar power plant for Jordan," *Journal of Cleaner Production,* vol. 17, no. 6, pp. 625-635, 2009.

[35] *ISCC Kuraymat* (n.d.) [Online]. Available: https://www.nrel.gov/csp/solarpaces/project_detail.cfm/projectID=65

[36] E. R. Shouman and N. Khattab, "Future economic of concentrating solar power (CSP) for electricity generation in Egypt," *Renewable and Sustainable Energy Reviews,* vol. 41, pp. 1119-1127, 2015.

[37] M. K. Patel, V. J. Patel, and A. M. Patel, "Modelling and simulation of CSP plant and analysis with grid integration," *International Journal For Technological Research In Engineering,* vol. 3, no. 2, pp. 303-310, 2015.

[38] S. Park. (2015). *Energy in Egypt: Backgrounds and issues* [Online]. Available: WWW.AmericanSecurityProject.org

[39] *The end of fossil fuels* (n.d.) [Online]. Available: https://www.ecotricity.co.uk/our-green-energy/energy-independence/the-end-of-fossil-fuels

[40] C. Tiba et al., "Siting study of solar thermoelectric plants in the state of Minas Gerais," *Journal of Geographic Information System,* vol. 6, no. 5, p. 423, 2014.

[41] G. C. Wu, R. Deshmukh, K. Ndhlukula, T. Radojicic, and J. Reilly, "Renewable energy zones for the Africa clean energy corridor," Lawrence Berkeley National Laboratory (LBNL), Berkeley, CA, 2015.

[42] *Direct normal irradiation map* (n.d.) [Online]. Available: https://solargis.com/maps-and-gis-data/download/egypt

[43] *Egypt – Topography* (n.d.) [Online]. Available: https://www.nationsencyclopedia.com/Africa/Egypt-TOPOGRAPHY.html

[44] *Elevation and elevation maps of cities/towns/villages in Egypt* (n.d.) [Online]. Available: http://www.floodmap.net/Elevation/CountryElevationMap/?ct=EG

[45] S. H. Mahmoud, A. Alazba, J. Adamowski, and A. El-Gindy, "GIS methods for sustainable stormwater harvesting and storage using remote sensing for land cover data-location assessment," *Environmental Monitoring and Assessment*, vol. 187, no. 9, p. 598, 2015.

[46] Transport Planning Authority and Japan International Cooperation Agency. (2012, March). The comprehensive study on the master plan for nationwide transport system in Egypt. [Online]. Available: http://open_jicareport.jica.go.jp/pdf/12057584.pdf

[47] Egyptian General Survey Authority. (2016). *Egypt's Road Network Map*. Egypt: Author.

[48] S. F. Elbeih, "An overview of integrated remote sensing and GIS for groundwater mapping in Egypt," *Ain Shams Engineering Journal*, vol. 6, no. 1, pp. 1-15, 2015.

[49] Egyptian Electricity Holding Company. (2016). Annual report [Online]. Available: http://www.moee.gov.eg/english_new/EEHC_Rep/2015-2016en.pdf

[50] Arab Union of Electricity. (2010). *Egypt's Electrical Network Map*. Egypt: Author.

[51] S. M. Romero. (n.d.). *CSP: Solar resource assessment* [Online]. Available: https://www.esmap.org/sites/default/files/esmap-files/ESMAP_IFC_RE_CSP_Training_World_Bank_Romero.pdf

[52] Google Maps. (2017). Google Maps: Egypt [Online]. Available at: https://www.google.com/maps/place/Egypt/@26.8349316,26.3816329,1547899m/data=!3m1!1e3!4m5!3m4!1s0x14368976c35c36e9:0x2c45a00925c4c444!8m2!3d26.820553!4d30.802498

[53] *Egypt's population density map* (n.d.) [Online]. Available: http://martinsidwell.com/wp-content/uploads/2015/04/Egypt-Population-Density.jpg

[54] *Shams 1* (n.d.) [Online]. Available: https://www.nrel.gov/csp/solarpaces/project_detail.cfm/projectID=69

[55] *Solnova 4* (n.d.) [Online]. Available: https://www.nrel.gov/csp/solarpaces/project_detail.cfm/projectID=25

[56] Remund, J. and S. Müller, *Meteonorm: Global Meteorological Database, Part 1: Software, Version 7.* Bern, Switzerland: Meteotest, 2007.

[57] Philibert, C. (2010). *Technology roadmap: Concentrating solar power, OECD/IEA* [Online]. Available: www.iea.org/about/copyright.asp

[58] *System Advisor Model Version 2017.9.5 (SAM 2017.9.5): User documentation, Single loop configuration ed*. National Renewable Energy Laboratory, Golden, CO, 2017.

[59] *Solar parabolic trough* (n.d.) [Online]. Available: https://www1.eere.energy.gov/ba/pba/pdfs/solar_trough.pdf

[60] *Siemens UVAC 2010,* Siemens AG, Nürnberg, Germany, 2010.

[61] W. Short , D.J. Packey and T. Holt, *A Manual for the Economic Evaluation of Energy Efficiency and Renewable Energy Technologies.* Golden, CO: National Renewable Energy Laboratory, 1995.

[62] *Inflation rate* (n.d.) [Online]. Available: https://www.focus-economics.com/economic-indicator/inflation-rate

[63] Renewable Energy Solutions for the Mediterranean. (2015). RES4MED country profiles (Egypt). RES4MED, Rome, Italy [Online]. Available: http://www.res4med.org/wp-content/uploads/2017/05/RES4MED-Day-Egypt-2015_Country-profile.pdf

[64] *Egypt raises energy prices hours after floating currency* (2016, Nov.) [Online]. Available: https://www.ft.com/content/f0773e66-a1a0-11e6-86d5-4e36b35c3550

[65] N. Hussein, M. Abokersh, Ch. Kost and T. Schlegl. (2016, Dec.). Electricity cost from renewable energy technologies in Egypt. Fraunhofer Institute for Solar Energy Systems ISE, Freiburg, Germany. [Online]. Available: https://www.ise.fraunhofer.de/content/dam/ise/en/documents/publications/studies/Dec2016_Fraunhofer- ISE_LCOE_Renewable_Energy_Technologies_EN_v20_ns.pdf

[66] U.S. Department of State (2015, May). Egypt investment climate statement. Federal Government of the United States [Online]. Available: https://www.state.gov/documents/organization/241756.pdf

[67] *Simulink and Simscape Power Systems Toolbox Release 2017b*, The MathWorks, Inc., Natick, MA, 2017.

[68] J. D. Glover, T. J. Overbye, and M. S. Sarma, *Power System Analysis & Design*, 6th ed. Boston, MA: Cengage Learning, 2017.

[69] P. Murty, *Power Systems Analysis,* 2nd ed. Oxford, UK: Butterworth-Heinemann, 2017.

[70] *Egypt technical information for travelers* (n.d.) [Online]. Available: https://www.voltageplugregion.com/egypt-technical-information-for-travelers.html

[71] J. Parmar. (2012, July). *Delta-Star transformer connection overview* [Online]. Available: http://electrical-engineering-portal.com/delta-star-transformer-connection-overview

[72] J. Parmar. (2012, June). *Star-Delta transformer connection overview* [Online]. Available: http://electrical-engineering-portal.com/star-delta-transformer-connection-overview

[73] E. Csanyi. (2016, June). *Purpose of grounding transformer* [Online]. Available: http://electrical-engineering-portal.com/grounding-transformer-zig-zag-grounded-wye-delta

[74] *Electrical power distribution* (n.d.) [Online]. Available: http://www.aast.edu/papers/staffcourses/45_16255_EE543_2015_1__1_1_week_1-2.pdf

[75] J. Parmar. (2012, May). *Transformer connection Star-Star* [Online]. Available: http://electrical-engineering-portal.com/transformer-connection-star-star

[76] *Power transformers*, Elsewedy Electric, Egypt, 2011.

[77] *Modeling of transmission lines* (n.d.) [Online]. Available: http://eee.guc.edu.eg/Courses/Electronics/ELCT908%20Distributed%20Power%20Systems/Lectures/Modeling%20of%20Transmission%20Lines.pdf

[78] *Design tool for measuring transmission and distribution parameters* (n.d.) [Online]. Available: http://www.alconesy2k17.com/#somethingonpage

[79] *Transmission lines* (n.d.) [Online]. Available: http://www.ee.unlv.edu/~eebag/EE%20340%20Transmission%20%20Lines.pdf

[80] W. S. I. Alsuraih. (2014). Integrated safeguards data sheet (restructuring stage) - Egypt - Wind power development project - P113416 (English). Washington, DC: World Bank Group. [Online]. Available: http://documents.worldbank.org/curated/en/889571468234333736/Integrated-Safeguards-Data-Sheet-Restructuring-Stage-Egypt-Wind-Power-Development-Project-P113416

[81] *EPRI AC transmission line reference book-200 kV and above*, 3rd ed., EPRI, Palo Alto, CA, 2005.

[82] *Aluminium Conductors Steel Reinforced (ACSR),* Midal Cable, Kingdom of Bahrain, n.d.

[83] *Aluminium Reinforced Conductors*, Prysmian Group, Auckland, New Zealand, 2017.

[84] *ACSR - ASTM - B Aluminium Conductor Steel Reinforced*, Eland Cables, London, UK, 2014.

[85] W. O. Kennedy. (2013, Jan). *Transmission lines: Electricity's highways* [Online]. Available: http://sites.ieee.org/sas-pesias/files/2016/03/IEEE_PES-IAS_Chapter_24_01_13.pdf

[86] *Overhead line (OHL) electrical parameters* (n.d.) [Online]. Available: https://www.powerwiki.cz/wiki/MainEn?language=en

[87] A. K. Akhani (2014,April). *Types of electric loads* [Online]. Available: http://top10electrical.blogspot.co.nz/2014/04/types-of-electric-loads.html

[88] V. Mehta and R. Mehta, *Principles of Power Systems,* New Delhi, India: S. Chand, 2011.

Appendix A: SAM Simulation Setups

The parameter values for each section of SAM for the three selected sites were set as shown in Figures (A. 1: A. 12). There were two parameter sections that had different values for each site. The first section was location and resources as each site has different coordinates. Also, the thermal storage settings were changed based on the different DNI values for each selected site. All other values were fixed for each case study.

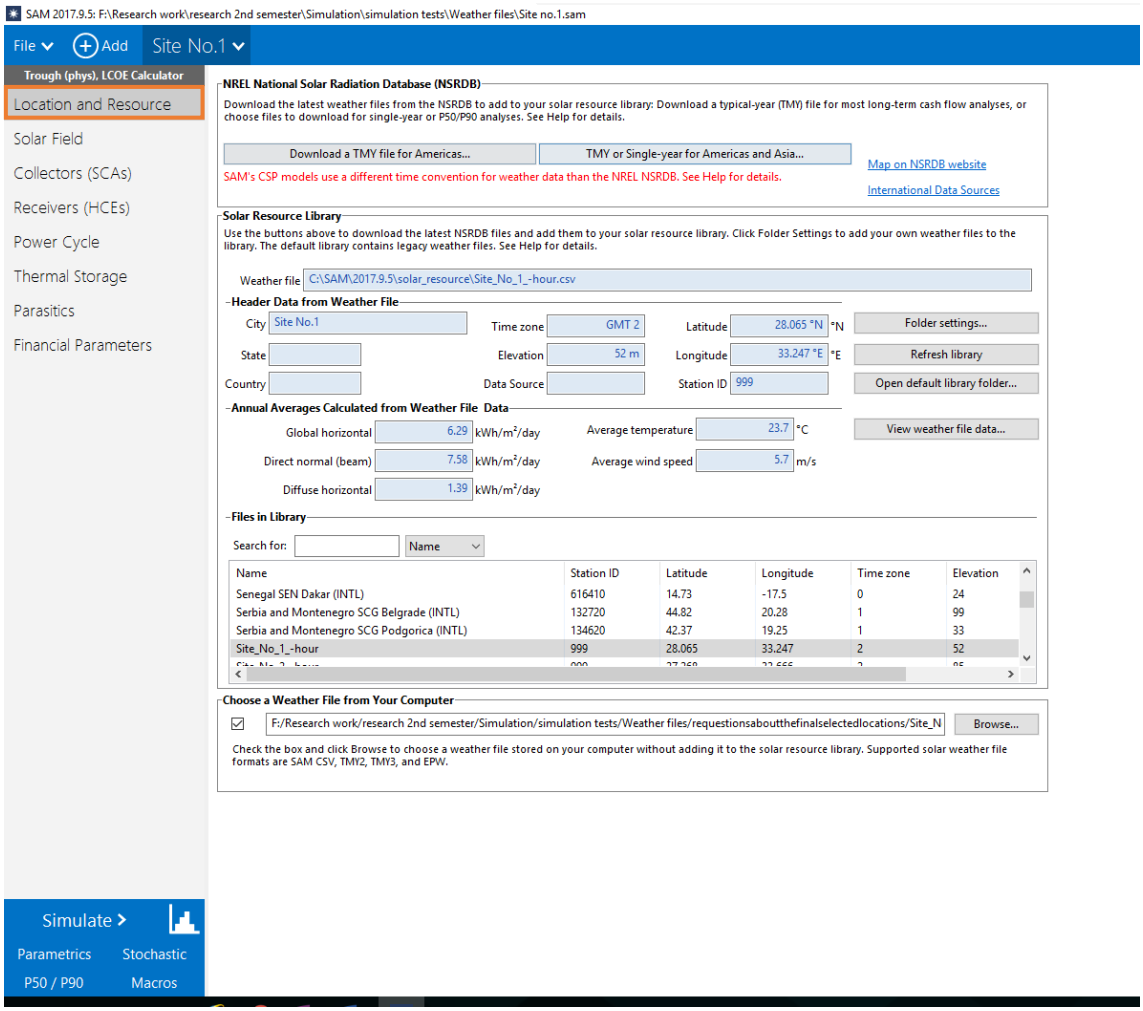

Figure (A. 1): Location and resource parameter settings for the first selected site.

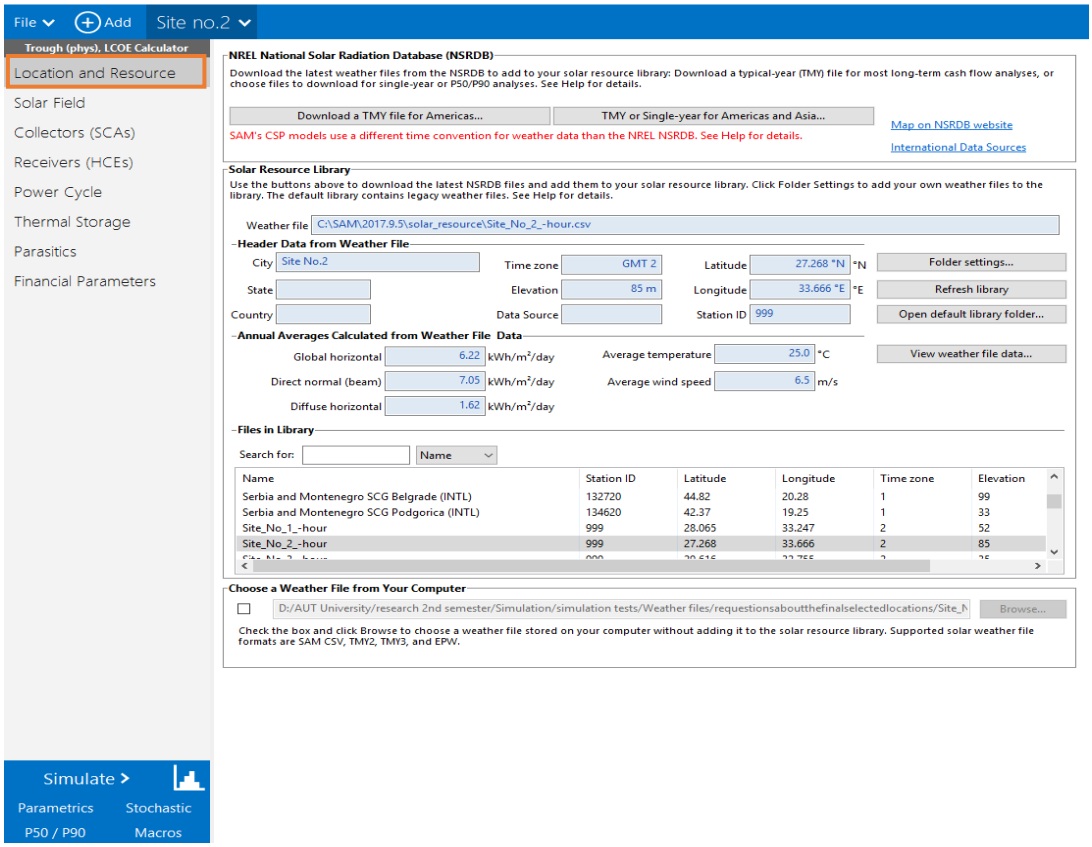

Figure (A. 2): Location and resource parameter settings for the second selected site.

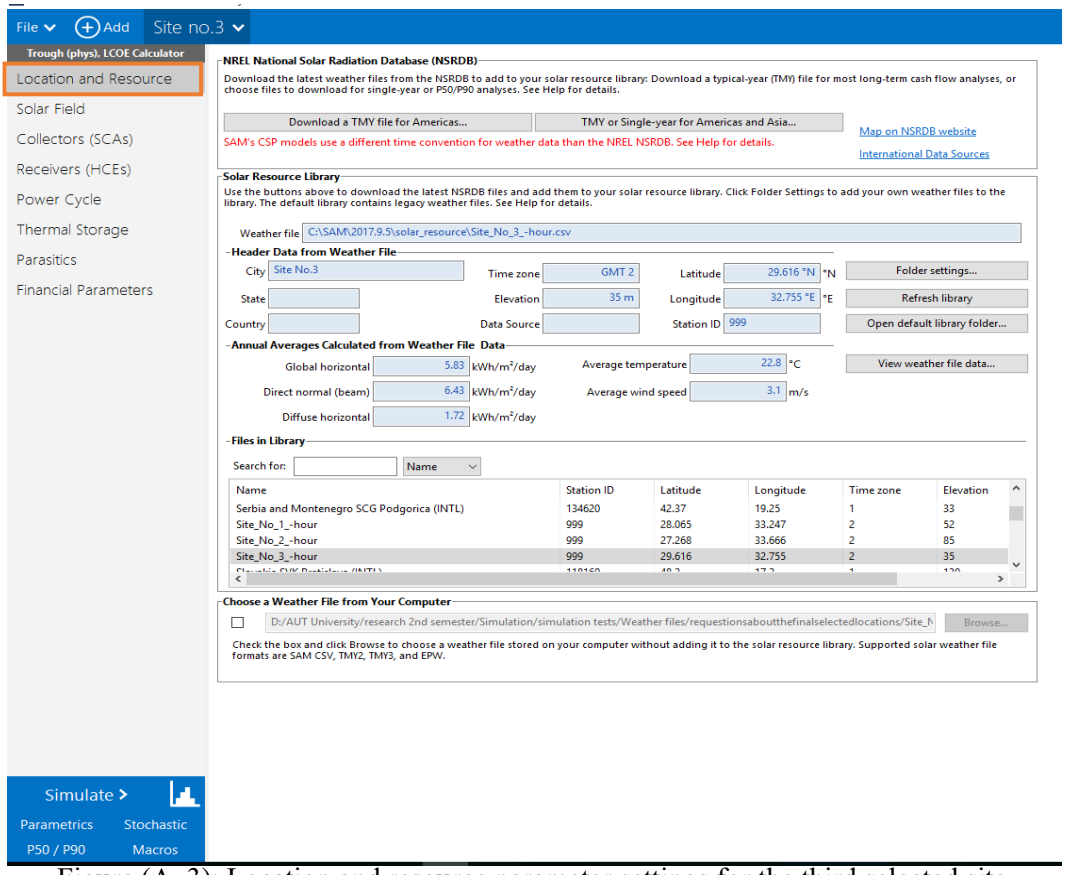

Figure (A. 3): Location and resource parameter settings for the third selected site.

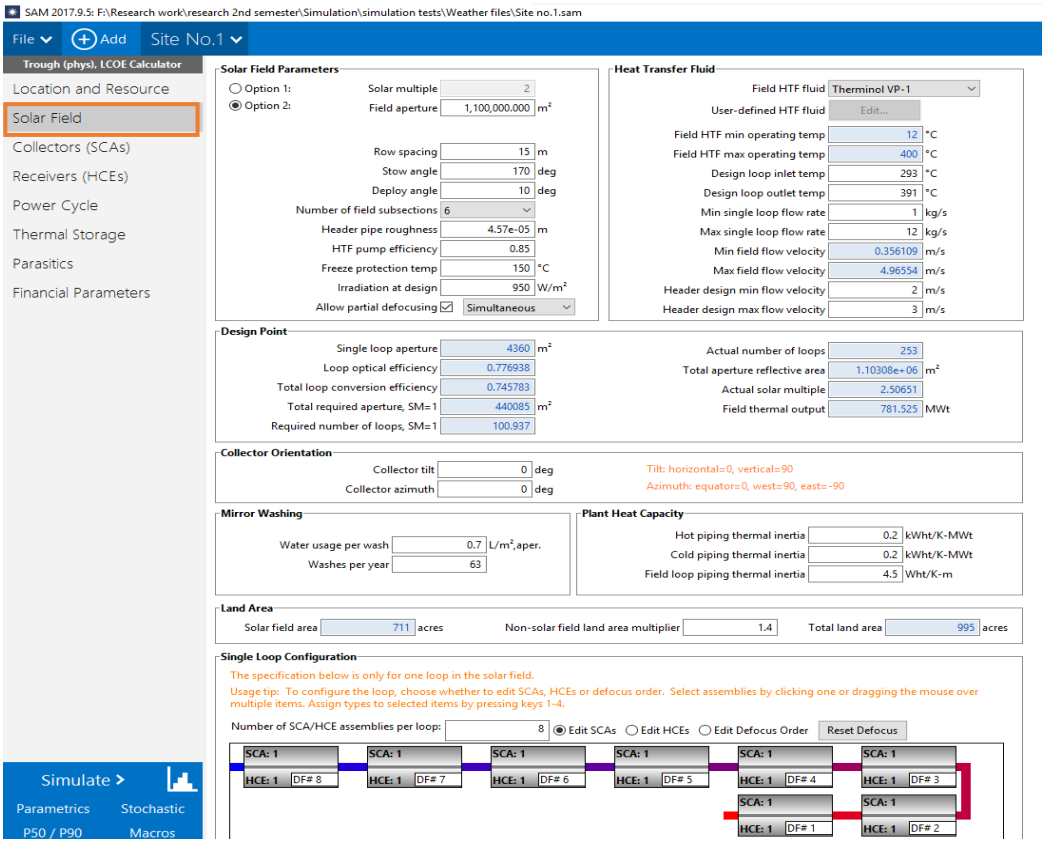

Figure (A. 4): Solar field parameter settings.

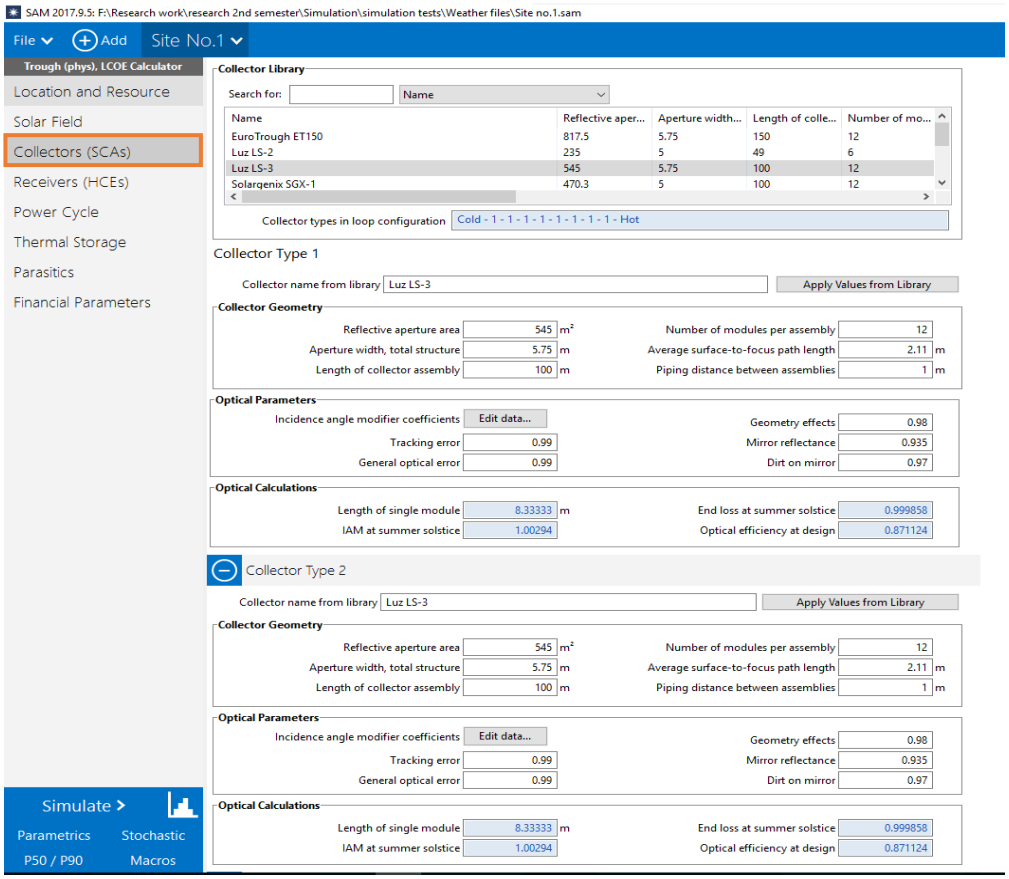

Figure (A. 5): Collectors' parameter settings.

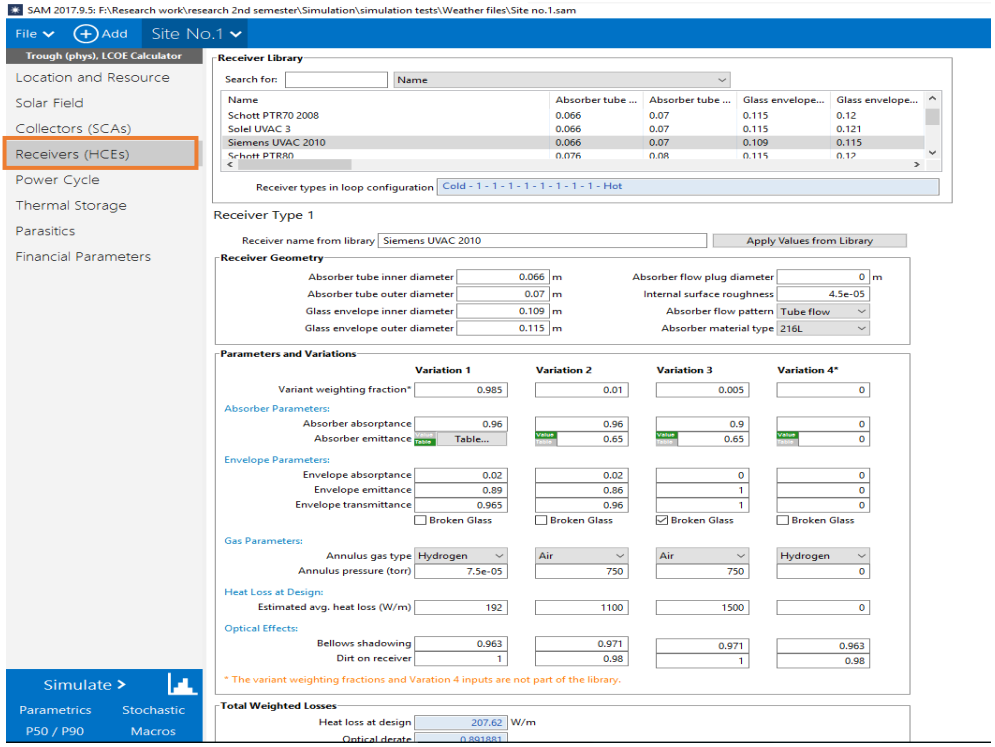

Figure (A. 6): Receivers' parameter settings.

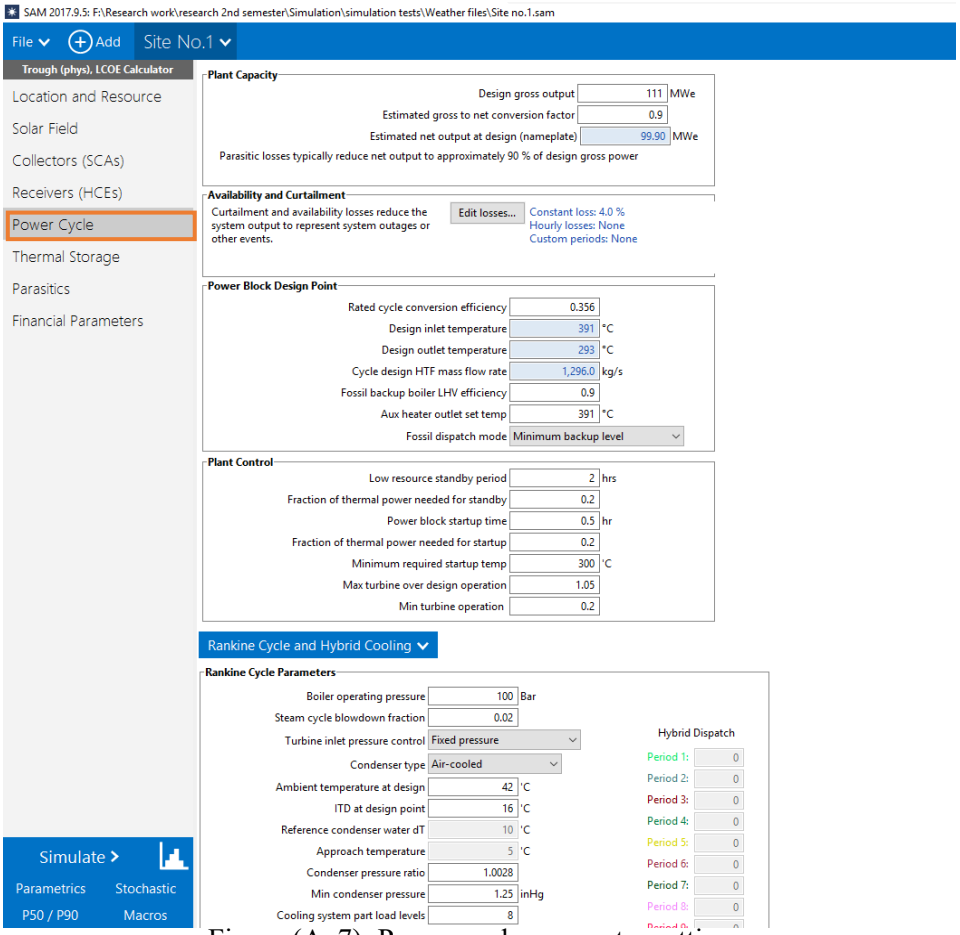

Figure (A. 7): Power cycle parameter settings.

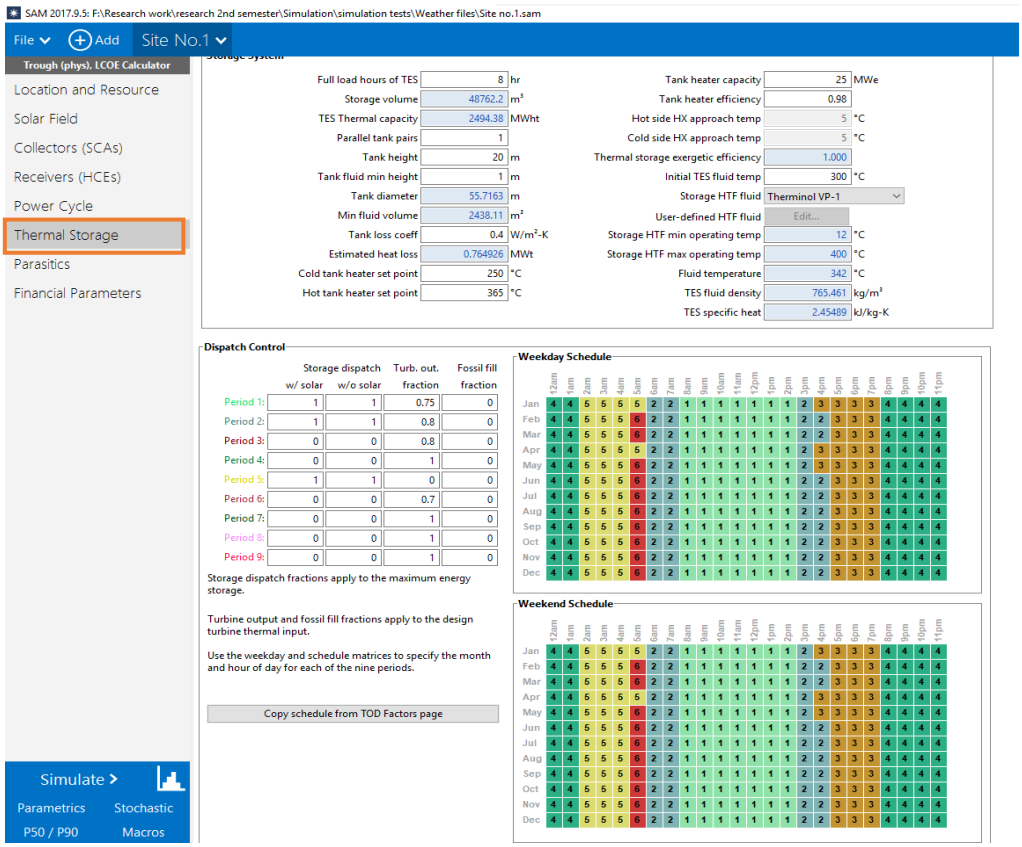

Figure (A. 8): Thermal storage parameter settings for the first selected site.

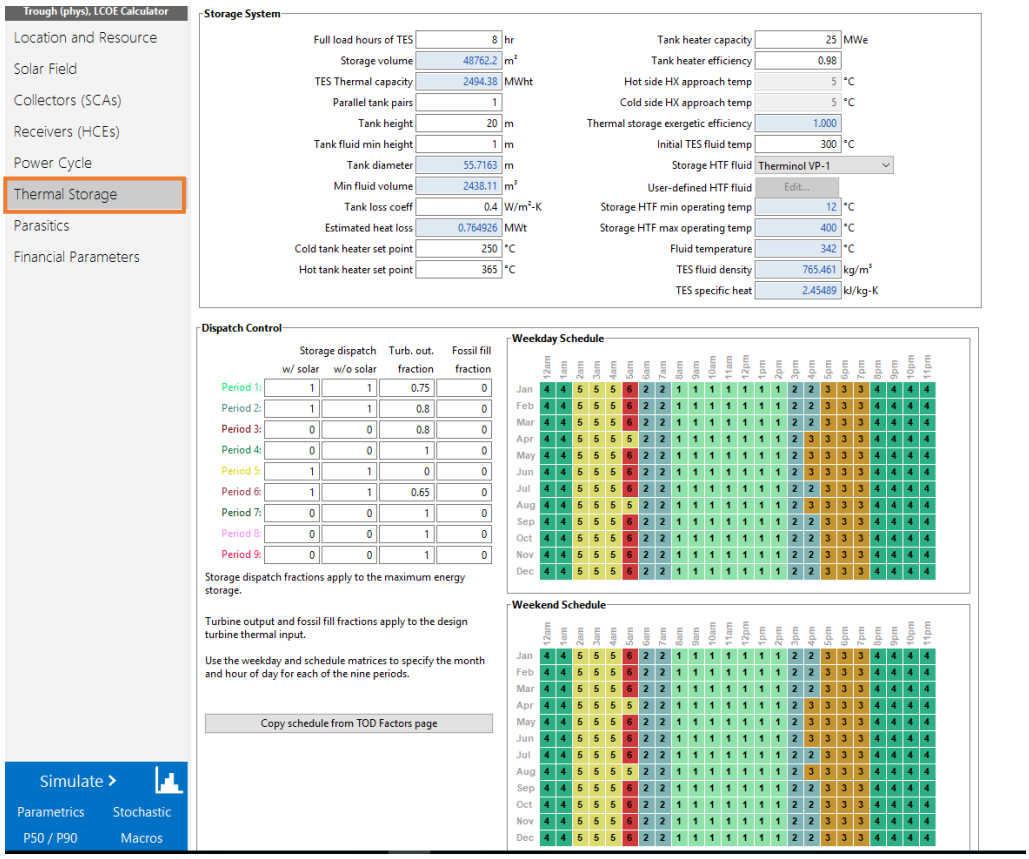

Figure (A. 9): Thermal storage parameter settings for the second selected site.

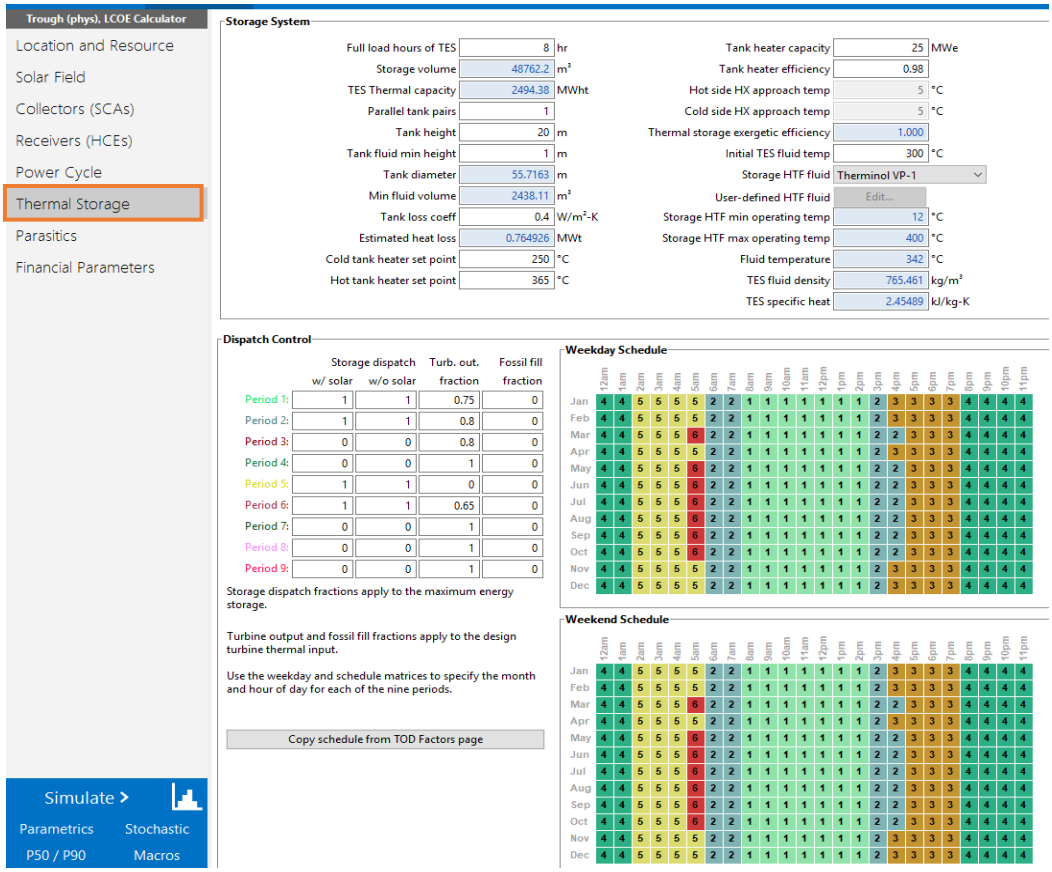

Figure (A. 10): Thermal storage parameter settings for the third selected site.

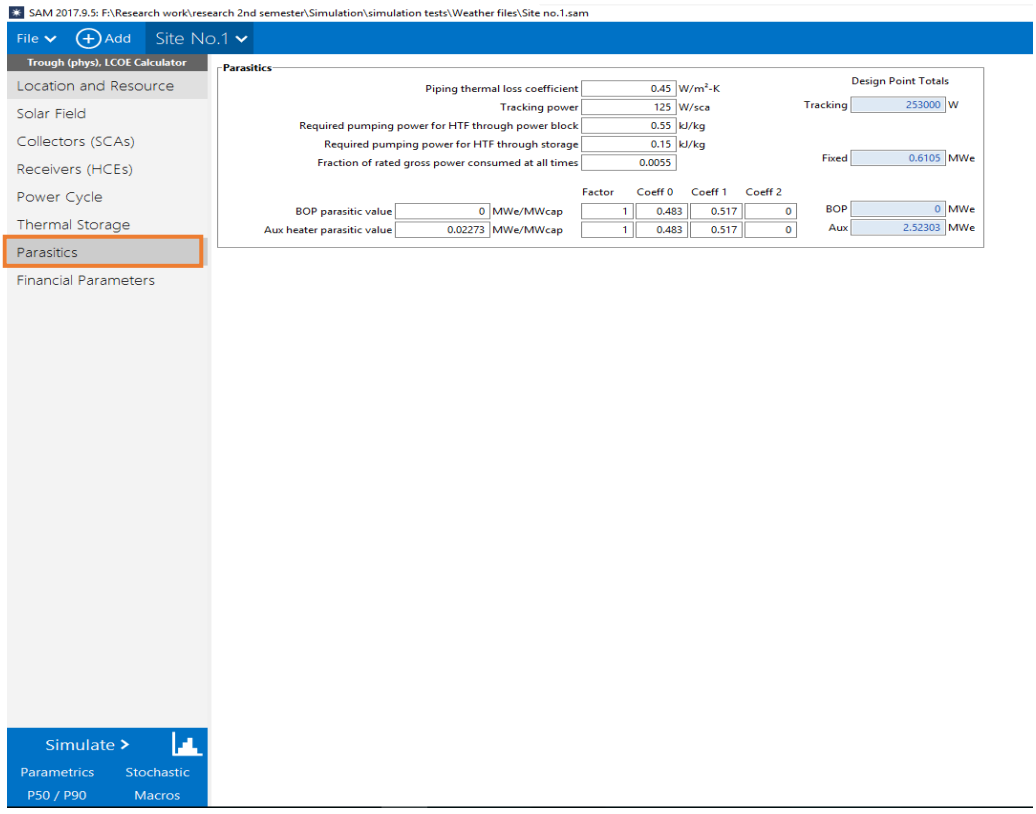

Figure (A. 11): Parasitics parameter settings.

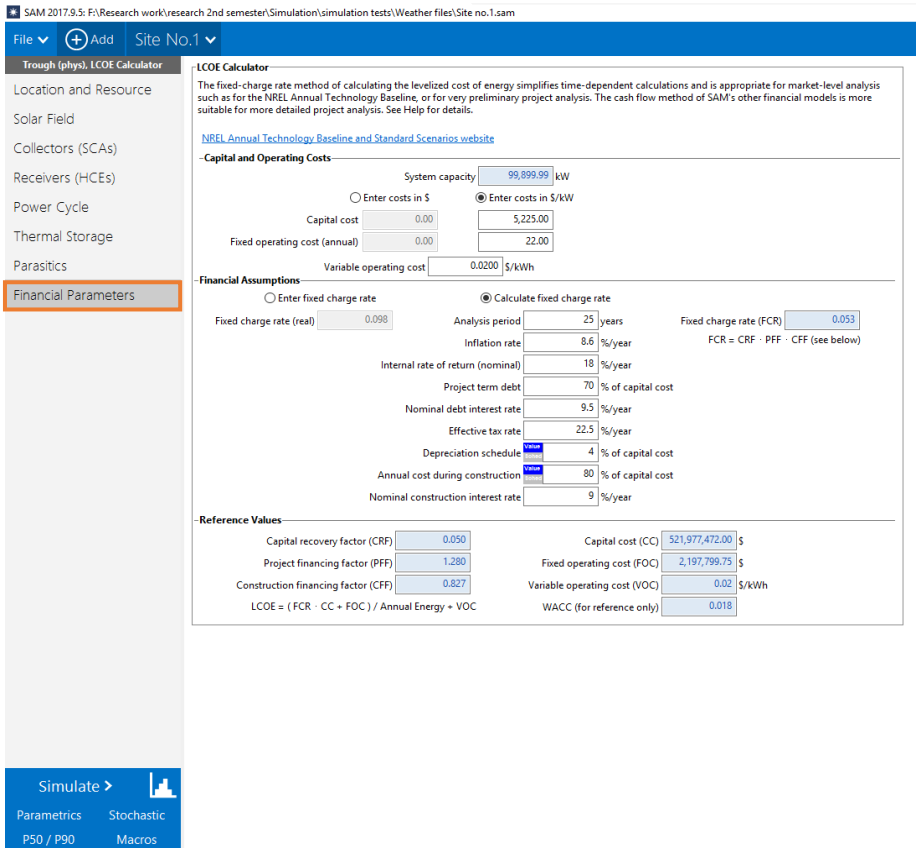

Figure (A. 12): Financial parameter settings.

Appendix B: Load Flow in Simulink and Results

After designing the Simulink model as shown in Figure (B.1), the powergui load flow tool was used to solve the load flow problem by performing positive sequence load flow. This tool uses a Newton Raphson algorithm for the solution. The general solver from the configuration parameters in Simulink should allow phasor simulation; hence, solver ode23tb was used for this purpose with variable step. The frequency was set as 50 Hz as the simulation was conducted in the case of steady state. The simulation process itself in Simulink can be conducted by two methods, either by accessing the power flow tool from Simulink or by accessing it through commands in MATLAB.

In the first method, after setting all the input data, the machine initialisation tool was used for setting the starting parameters for the synchronous generator block. As the simulation was conducted for every hour of generation and there are five values of zero generation from late at night to early morning. Consequently, the simulation was conducted 20 times not 24. For each simulation the active power value was changed according to the values of the hourly generated power. The final solution of the load flow each time was set as the machine initialisation mode for the next simulation process; and it should be noted that the synchronous generation started at zero for generated power at the first simulation attempt.

The second approach in conducting the simulation was by using commands through MATLAB to access Simulink. These commands open the same interface that was used in the first method and set the initial active power value for the synchronous generator (machine initialisation) and solve the load flow and initialise the model with the load flow solution for the next simulation. Finally, it computes the load flow and generates a report containing the results. The commands are shown in Figure B. 2 and the powergui load flow interface is shown in Figure B. 3.

As the simulation was conducted for 24 hours, the load flow solution showed the values for each hour during the day including the total generation, total losses, and all the p.u. values of voltage and voltage angles. In addition to these, the mechanical power input and field voltage were given. The results are shown in detail in Table B. 1.

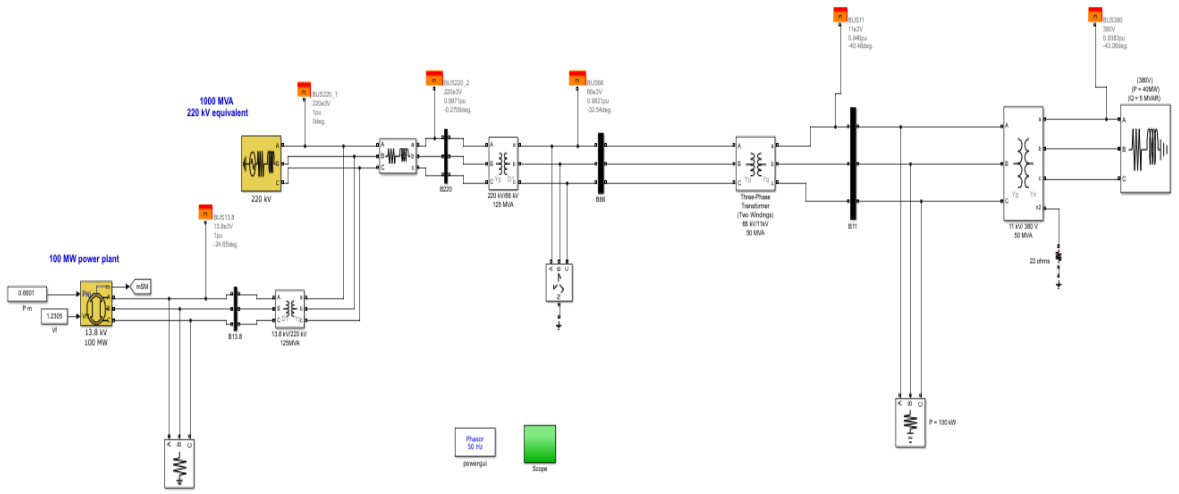

Figure (B.1): Simulink model of the proposed CSP plant's connection to the grid network.

```
Command Window
>> Mparam = power_loadflow('Modell');
>> Mparam(1).set

ans =

  struct with fields:

           BusType: 'P & V generator'
    TerminalVoltage: 13800
        ActivePower: 0
      ReactivePower: 0
           PhaseUan: 0

>> LF = power_loadflow('-v2','Modell');
>> LF = power_loadflow('-v2','Modell','solve');
>> LF = power_loadflow('-v2','Modell','solve','report');
fx >>
```

Figure (B. 2): The commands used for accessing the powergui load flow tool in MATLAB.

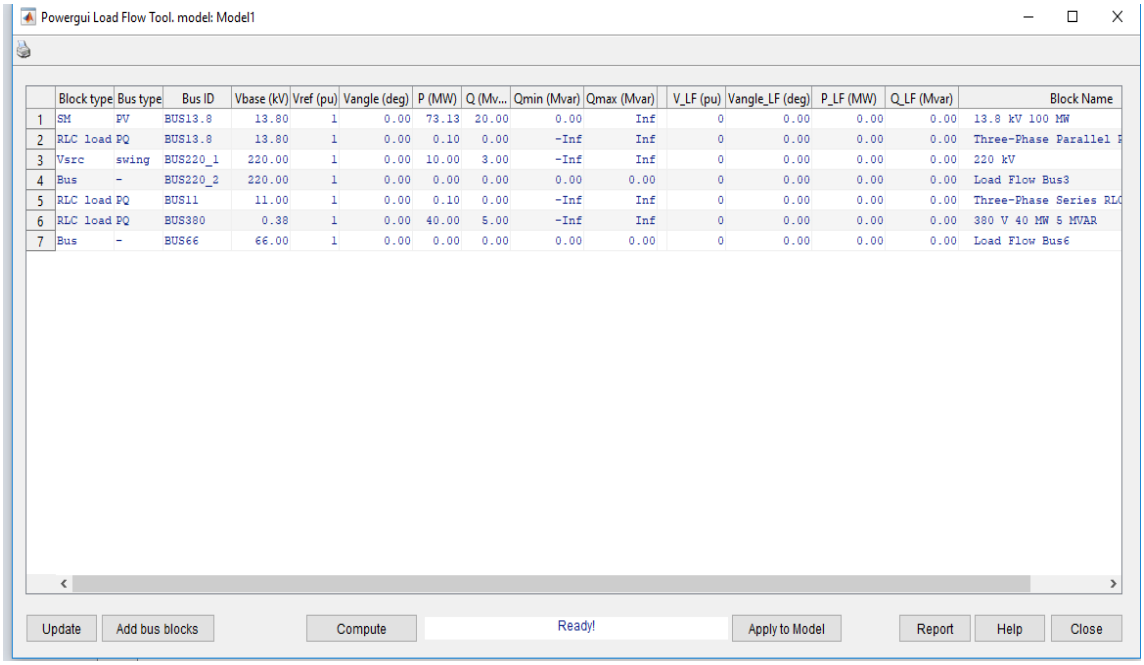

	Block type	Bus type	Bus ID	Vbase (kV)	Vref (pu)	Vangle (deg)	P (MW)	Q (Mv...	Qmin (Mvar)	Qmax (Mvar)	V_LF (pu)	Vangle_LF (deg)	P_LF (MW)	Q_LF (Mvar)	Block Name
1	SM	PV	BUS13.8	13.80	1	0.00	73.13	20.00	0.00	Inf	0	0.00	0.00	0.00	13.8 kV 100 MW
2	RLC load	PQ	BUS13.8	13.80	1	0.00	0.10	0.00	-Inf	Inf	0	0.00	0.00	0.00	Three-Phase Parallel
3	Vsrc	swing	BUS220_1	220.00	1	0.00	10.00	3.00	-Inf	Inf	0	0.00	0.00	0.00	220 kV
4	Bus	-	BUS220_2	220.00	1	0.00	0.00	0.00	0.00	0.00	0	0.00	0.00	0.00	Load Flow Bus3
5	RLC load	PQ	BUS11	11.00	1	0.00	0.10	0.00	-Inf	Inf	0	0.00	0.00	0.00	Three-Phase Series RL
6	RLC load	PQ	BUS380	0.38	1	0.00	40.00	5.00	-Inf	Inf	0	0.00	0.00	0.00	380 V 40 MW 5 MVAR
7	Bus	-	BUS66	66.00	1	0.00	0.00	0.00	0.00	0.00	0	0.00	0.00	0.00	Load Flow Bus6

Figure (B. 3): The powergui load flow tool interface showing the load bus data.

Table (B. 1): Results of the load flow solution.

Hours	Total generation	Total PQ load	Total losses	Swing bus P & Q	CSP P &Q	Voltage (p.u.) and angle (deg)					No. of iterations	P mechanical (p.u.)*	Vf (p.u.)*
						Bus 13.8	Bus 220	Bus 66	Bus11 (load)	Bus 380 (load)			
1	41.50 MW/ 20.18 MVAR	40.20 MW /5.00 MVAR	0.43 MW /14.40 MVAR	-18.04 MW /19.28 MVAR	59.54 MW/ 0.90 MVAR	1/ -25.65°	1 / 0°	0.982/ -32.54°	0.946 / -40.48°	0.938 / -43.06°	2	0.54	1.15
2	41.41 MW 16.51 MVAR	40.20 MW/ 5.00 MVAR	0.34 MW/ 10.73 MVAR	15.68 MW/ 16.60 MVAR	25.72 MW/ 0 MVAR	1/ -28.13°	1/ 0°	0.982/-32.54	0.946 / -40.48°	0.938 / -43.06°	2	0.23	1.03
3	41.39 MW 15.68 MVAR	40.20 MW /5.00 MVAR	0.32 MW /9.9 MVAR	41.39 MW/ 15.55 MVAR	0MW/ 0 MVAR	1 / -30.02°	1 / 0°	0.982/ -32.54°	0.946 / -40.48°	0.938 / -43.06°	2	0	0
4	41.39 MW 15.68 MVAR	40.20 MW /5.00 MVAR	0.32MW /9.9 MVAR	41.39 MW/ 15.55 MVAR	0MW/ 0 MVAR	1/ -30.02°	1 / 0°	0.982/ -32.54°	0.946 / -40.48°	0.938 / -43.06°	5	0	0

Table (B.1): Results of the load flow solution (continued).

Hours	Total generation	Total PQ load	Total losses	Swing bus P & Q	CSP P &Q	Voltage (p.u.) and angle (deg)					No. of iterations	P mechanical (p.u.)*	Vf (p.u.)*
						Bus 13.8	Bus 220	Bus 66	Bus11 (load)	Bus 380 (load)			
5	41.39 MW/ 15.68 MVAR	40.20 MW / 5.00 MVAR	0.32 MW / 9.9 MVAR	41.39 MW/ 15.55 MVAR	0MW/ 0 MVAR	1 / -30.02°	1 / 0°	0.982 / -32.54	0.946 / -40.48°	0.938/- 43.06°	2	0	0
6	41.39 MW/ 15.68 MVAR	40.20MW/ 5.00 MVAR	0.32 MW / 9.9 MVAR	41.39 MW/ 15.55 MVAR	0MW / 0 MVAR	1 / -30.02°	1/ 0°	0.982 / -32.54	0.946 / -40.48°	0.938/- 43.06°	2	0	0
7	41.39 MW/ 15.68 MVAR	40.20MW/ 5.00 MVAR	0.32 MW / 9.9 MVAR	41.39 MW/ 15.55 MVAR	0MW/ 0 MVAR	1/ -30.02°	1/ 0°	0.982 / -32.54	0.946 / -40.48°	0.938/- 43.06°	2	0	0
8	41.39 MW /15.95 MVAR	40.20MW/ 5.00 MVAR	0.32 MW /10.17 MVAR	26.66 MW 16.05 MVAR	14.73 MW/ 0.00 MVAR	1 / -28.94°	1/ 0°	0.982 / -32.54	0.946 / -40.48°	0.938/- 43.06°	2	0.133	1.008
9	41.46 MW / 18.49 MVAR	40.2 MW/ 5.00 MVAR	0.39 MW/ 12.71 MVAR	-5.64 MW 18.13 MVAR	47.10MW/ 0.36 MVAR	1/ -26.56°	1/ 0°	0.982 / -32.54	0.946 / -40.48°	0.938/- 43.06°	2	0.425	1.095

Table (B.1): Results of the load flow solution (continued).

Hours	Total generation	Total PQ load	Total losses	Swing bus P & Q	CSP P &Q	Voltage (p.u.) and angle (deg)					No. of iterations	P mechanical (p.u.)*	Vf (p.u.)*
						Bus 13.8	Bus 220	Bus 66	Bus11 (load)	Bus 380 (load)			
10	41.54 MW/ /21.82 MVAR	40.2MW/ 5.00 MVAR	0.47MW/ 16.04 MVAR	-27.93 MW /20.35 MVAR	69.47 MW / 1.47 MVAR	1/ -24.92°	1/ 0°	0.982 / -32.54°	0.946 / -40.48°	0.938/- 43.06°	2	0.627	1.208
11	41.56 MW/ 22.71 MVAR	40.2MW/ 5.0 MVAR	0.49 MW /16.93 MVAR	-32.76 MW/ 20.91 MVAR	74.32 MW/ 1.80 MVAR	1 / -24.56°	1/ 0°	0.982 / -32.54°	0.946 / -40.48°	0.938/- 43.06°	2	0.671	1.238
12	41.56 MW/ 22.67 MVAR	40.2MW/ 5.0 MVAR	0.5 MW/ 16.89 MVAR	-32.42 MW/ 20.89 MVAR	74.14 MW/ 1.78 MVAR	1/ -24.57°	1/ 0°	0.982 / -32.54°	0.946 / -40.48°	0.938/- 43.06°	2	0.669	1.237
13	41.56 MW / 22.71 MVAR	40.20 MW/ 5.00 MVAR	0.49 MW /16.93 MVAR	-32.78 MW 21.02 MVAR	74.34 MW/ 1.80 MVAR	1/ -24.56°	1/ 0°	0.982 / -32.54°	0.946 / -40.48°	0.938/- 43.06°	2	0.671	1.238
14	41.56 MW/ 22.88 MVAR	40.20 MW 5.00 MVAR	0.5 MW/ 17.09 MVAR	-33.63 MW 21.02 MVAR	75.20 MW/ 1.86 MVAR	1/ -24.50°	1 / 0°	0.982 / -32.54°	0.946 / -40.48°	0.938/- 43.06°	2	0.679	1.244

Table (B. 1): Results of the load flow solution (continued).

Hours	Total generation	Total PQ load	Total losses	Swing bus P & Q	CSP P &Q	Voltage (p.u.) and angle (deg)					No. of iterations	P mechanical (p.u.)*	Vf (p.u.)*
						Bus 13.8	Bus 220	Bus 66	Bus11 (load)	Bus 380 (load)			
15	41.57 MW 23.05 MVAR	40.20 MW /5.00 MVAR	0.5 MW/ 17.27 MVAR	-34.52 MW/ 21.13 MVAR	76.09 MW /1.92 MVAR	1/ -24.43°	1/ 0°	0.982 / -32.54°	0.946 / -40.48°	0.938/- 43.06°	2	0.687	1.249
16	41.60 MW/ 24.16 MVAR	40.20 MW /5.00 MVAR	0.53 MW/ 18.38 MVAR	-39.99 MW/ 21.82 MVAR	81.59 MW 2.34 MVAR	1/ -24.03°	1 / 0°	0.982 / -32.54°	0.946 / -40.48°	0.938/- 43.06°	2	0.737	1.286
17	41.53 MW/ 21.47 MVAR	40.20 MW /5.00 MVAR	0.46 MW/ 15.69 MVAR	-25.98 MW /20.13 MVAR	67.51 MW/ 1.35 MVAR	1/ -25.06°	1/ 0°	0.982 / -32.54°	0.946 / -40.48°	0.938/- 43.06°	2	0.609	1.197
18	41.55 MW/ 22.35 MVAR	40.20 MW /5.00 MVAR	0.48 MW / 16.57 MVAR	-30.87 MW 20.69 MVAR	72.42 MW 1.67 MVAR	1 / -24.70°	1/ 0°	0.982 / -32.54°	0.946 / -40.48°	0.938/- 43.06°	2	0.65372	1.2262

Table (B. 1): Results of the load flow solution (continued).

Hours	Total generation	Total PQ load	Total losses	Swing bus P & Q	CSP P &Q	Voltage (p.u.) and angle (deg)					No. of iterations	P mechanical (p.u.)*	Vf (p.u.)*
						Bus 13.8	Bus 220	Bus 66	Bus11 (load)	Bus 380 (load)			
19	41.55 MW/ 22.31 MVAR	40.20 MW 5.00 MVAR	0.48 MW/ 16.53 MVAR	-30.64 MW/ 20.66 MVAR	72.19 MW /1.65 MVAR	1/ -24.72°	1/ 0°	0.982 / -32.54°	0.946 / -40.48°	0.938/- 43.06°	2	0.651	1.225
20	41.55 MW/ 22.21 MVAR	40.20 MW /5.00 MVAR	0.48 MW / 16.43 MVAR	-30.12 MW/ 20.60 MVAR	71.67 MW /1.62 MVAR	1/ -24.76°	1/ 0°	0.982 / -32.54°	0.946 / -40.48°	0.938/- 43.06°	2	0.647	1.222
21	41.63MW /25.43 MVAR	40.20 MW /5.00 MVAR	0.56 MW/ 19.65 MVAR	-45.85 MW/ 22.60 MVAR	87.48 MW/ 2.83 MVAR	1/ -23.59°	1/ 0°	0.982 / -32.54°	0.946 / -40.48°	0.938/- 43.06°	2	0.789	1.327
22	41.60 MW /24.31 MVAR	40.20 MW / 5.00 MVAR	0.53 MW /18.53 MVAR	-40.73 MW/ 21.91 MVAR	82.33 MW / 2.40 MVAR	1/ -23.97°	1/ 0°	0.982 / -32.54°	0.946 / -40.48°	0.938/- 43.06°	2	0.743	1.291

Table (B.1): Results of the load flow solution (continued).

Hours	Total generation	Total PQ load	Total losses	Swing bus P & Q	CSP P &Q	Voltage (p.u.) and angle (deg)					No. of iterations	P mechanical (p.u.)*	Vf (p.u.)
						Bus 13.8	Bus 220	Bus 66	Bus11 (load)	Bus 380 (load)			
23	41.58 MW/ 23.30 MVAR	40.20 MW/ 5.00 MVAR	0.51 MW 17.52 MVAR	-35.82 MW 21.29 MVAR	77.39 MW / 2.02 MVAR	1 / -24.33°	1/ 0°	0.982 / -32.54°	0.946 / -40.48°	0.938/- 43.06°	2	0.699	1.258
24	41.55 MW/ 22.48 MVAR	40.20 MW /5.00 MVAR	0.49 MW/ 16.7 MVAR	-31.57 MW /20.77 MVAR	73.13 MW / 1.71 MVAR	1/ -24.65°	1/ 0°	0.982 / -32.54°	0.946 / -40.48°	0.938/- 43.06°	2	0.66	1.231

*Both the field voltage and the mechanical power input values were obtained during the load flow analysis using the value of the active output power based on SAM results.